Vision rescue via chemically engineered endogenous retinal ganglion cells.

Rana Muhammad Shoaib[1,2], Aregnazan Sandrosyan[1] and Biraj Mahato[1,2]*

[1]Cell Reprogramming Laboratory, Department of Surgery, Division of Ophthalmology, Children's Hospital Los Angeles, CA, USA.

[2]Department of Ophthalmology, Keck School of Medicine, University of Southern California, USA.

* To whom correspondence should be addressed:

Biraj Mahato, Department of Surgery, Division of Ophthalmology, Children's Hospital Los Angeles, 4650 Sunset Blvd, Los Angeles, California, CA 90027; Tel (323) 361- 8414.

Email: bmahato@chla.usc.edu

Abstract:

Loss of retinal ganglion cells (RGCs) is the final common end point for many optic neuropathies, ultimately leading to irreversible vision loss. Endogenous RGC regeneration from Müller cells presents a promising approach to treat these diseases, but mammalian retinas lack regenerative capacity. Here, we report a small molecule cocktail that causes endogenous Müller cell proliferation, migration, and specification to newly generated chemically induced RGCs (CiRGCs) in NMDA injured mice retina. Notably, regenerated CiRGCs extend axons towards optic nerve, and rescue vision post- NMDA treatment. Moreover, we successfully reprogrammed human primary Müller glia and fibroblasts into CiRGCs using this chemical-only approach, as evidenced by RGC-specific gene expression and chromatin signature. Additionally, we show that interaction between SOX4 and NF-kB determine CiRGC fate from Müller cells. We anticipate endogenous CiRGCs would have therapeutic potential in rescuing vision for optic nerve diseases.

Keywords: Müller glia, chemical reprogramming, chemically induced RGCs, small molecules, endogenous regeneration, vision restoration.

Background:

The regenerative capacity of the adult mammalian central nervous system, including the neurosensory retina, is limited [1-3]. However, recent research has shown that Müller glia, a type of support cell in the retina, can be reprogrammed into retinal neurons *in vivo* [4-8]. In lower vertebrates, Müller glia naturally transforms into neural progenitor cells and generate functional neurons to restore vision after injury. Researchers are currently addressing the limitation of endogenous mammalian retinal neurogenesis in two main ways: i) transplanting *in vitro* engineered stem cell derived retinal neurons or neural progenitor cells into injured retina[9-15] or ii) overexpression of transcription factors in Müller cells to regenerate neural progenitors or retinal neurons to restore retinal function[16-22]. However, these methods involve the use of viruses which present challenges for its clinical implementation. An alternative method, using small molecules for chemical reprogramming, has recently garnered considerable attention [23-26]. In a prior study, we demonstrated that a combination of five small molecules (referred to as 5C) could reprogram fibroblasts into photoreceptors, subsequently leading to vision restoration upon subretinal transplantation in blind mice[27]. By augmenting 5C with supplementary molecules, here we report a chemical combination that stimulates proliferation, migration, and trans-differentiation of resident retinal Müller cells into CiRGCs after NMDA-induced RGC damage. To validate the Müller origin of CiRGCs, we conducted lineage tracing experiments using two mouse models. Moreover, regenerated CiRGCs pass axons through the optic nerve head and rescued vision in the NMDA injured mice. Lastly, we furnish supplementary evidence by demonstrating that human primary Müller glia and fibroblasts can also be reprogrammed into CiRGCs *in vitro* using a similar chemically induced approach.

Results:

Chemical cocktail induces endogenous Müller glia to become CiRGCs in NMDA-injured retina.

Based on our previous work[27], we tested if 5C [Valproic acid (V), CHIR (C), Repsox (R), Forskolin (F), and IWR1 (I)] along with additional chemicals or factors can induce endogenous Müller cell proliferation and subsequent retinal neurogenesis in NMDA

mediated RGC degeneration**.** We found 5C plus Noggin and IGF1 (2F) along with an additional molecule S24795 (hence 6C+2F) can induce Müller cell proliferation in the inner nuclear layer (INL) and migration to ganglion cell layer (GCL) after NMDA injury (with 75%-85% RGC loss) (**Fig. 1**, **Extended data Fig. 1a-d, Extended data Table 1, 2**). Müller cell proliferation and migration was examined on day 1,2, 3 and 6 based on prior research (**Fig. 1a**).[28, 29] On day 1, $BrdU^+$ cells were evident along the outer edge of INL in NMDA injured retina similar to published studies (**Fig. 1b**) [6, 29]. These $BrdU^+$ cells were also colocalized with Müller marker glutamine synthetase (GS) (**Fig. 1c, d**)[30, 31]. By contrast no $BrdU^+$ cells were observed at the same layer in vehicle injected eyes (**Extended data Fig. 2a-d**). On day 3, $BrdU^+$ (approx. 39.13±2.7%) cells were located along the GCL that indicates cell migration (**Fig.1e, f)**. When stained with SNCG, a RGC specific marker, we found 30±1.7% of cells in GCL layer are $SNCG^+$ $BrdU^+$ (**Fig. 1g, h**). Taken together, these data suggest that 6C+2F can induce endogenous Müller glia proliferation, migration, and differentiation into CiRGCs.

Endogenous CiRGCs are of Müller origin and extend axons to the optic nerve.

Next, we lineage traced CiRGCs by intravitreally injecting AAV2-GLAST-GFP into WT (C57/BL6, control) and NMDA injured mice (approx.10^6 vg/eye) before cocktail injection (**Fig. 2a**). 7 days after AAV2 injection, we observed specific GFP expression in Müller cells of WT retina, while almost no GFP was detectable in GCL (**Extended data Fig. 3a-c**). After administering 6C+2F into AAV2 injected mice eye, we found GFP^+BrdU^+ cells on the inner side of INL layer on day1 and on the GCL layer on day3 (approx. 35%±6.1 GFP^+BrdU^+ cells) (**Fig. 2b, d, e**). The expression of GFP in $BrdU^+$ cells at INL indicated their origin from Müller cells (**Fig. 2b, middle, white boxes**). Furthermore, we observed GFP^+RBPMS^+ cells on day-3-retinal sections which further supports Müller origin of CiRGCs (**Fig. 2c, f**). Additionally, we used a GLAST-CreERT2;ROSA26-flox-stop-flox (Ai9) mice that specifically express TdTomato in Müller cells and allowed us to track their fate following NMDA-damage (**Fig. 3a**). We found $RBPMS^+$ $TdTomato^+$ RGCs in GCL in cocktail treated but not in PBS treated eyes on day3 (**Fig. 3b, c, Extended data Fig. 4a, b**). These findings confirmed the Müller cell origin of CiRGCs.

Next, we investigated if Tdtomato$^+$ CiRGCs projected axons to the optic nerve, an essential step for vision rescue. Absence of TdTomato$^+$ axons in GLAST-Cre;TdTomato optic nerve upon NMDA injury (without cocktail) indicated suitability of this model for the study (**Fig. 3d**). Subsequently we found TdTomato$^+$ axons are passed through the optic nerve head in cocktail treated but not PBS treated eyes on day 6 (**Fig. 3e)**. We observed severely damaged RGC axons and reduced intensity of TUBB3 (15.5% of WT) staining in the optic nerve following NMDA treatment which was recovered after cocktail treatment (29.6% of WT) (**Fig. 3e, left panels, Extended data Fig. 4c**). Further analysis of cocktail treated eyes indicated expression of TUBB3 (axonal marker) in TdTomato$^+$ axons that are passed to the proximal part of the optic nerve via optic nerve head (**Fig. 3e-h, Extended data Fig. 4d-f**)[32]. These results suggested that endogenously regenerated CiRGCs extend their axons to the proximal part of the optic nerve through optic nerve head.

Endogenous CiRGCs rescue vision after NMDA mediated RGC damage.

To address the paramount question of whether CiRGC regeneration leads to vision rescue, we measured electrical activity from retina and visual cortex of the brain using pattern ERG (pERG) and pattern VEP (pVEP) following the scheme in **Fig. 4a.** We observed pERG and pVEP rescue starting from day 16, after that day 23, day 30 & day 60 in cocktail treated eyes compared to vehicle (**Fig. 4b, c**). pERG and pVEP amplitudes were rescued to 63% and 89% of the baseline respectively on day 60. We noted differential improvement between right and left eyes both in pERG (right 59% vs left 35.2%) and pVEP (right 81% vs left 58.7%) until day 23. This difference becomes narrower (pERG; right, 56%, left 51%, pVEP; right, 96.8%, left,73.5%) on day 30. Next, we conducted a longitudinal light avoidance test in the pERG & pVEP rescued animals following published methods to determine whether improved retinal function is sufficient to rescue visually evoked behaviour[33-35]. Normal mice exhibit a natural aversion to brightly illuminated areas, forming the basis for this test. All animals were placed in the apparatus for a duration of 300 seconds, and the proportion of time spent in the brightly lit (2800 lux, similar to cloudy outdoor environment) area was recorded. Wild type mice demonstrated a distinct preference for the dark compartment, while NMDA-treated mice did not display

such a preference (Mean: 195 ± 32 seconds versus 120 ± 29 seconds). Intriguingly, mice treated with cocktail exhibited a clear and statistically significant preference for the dark compartment (215 ± 37 seconds) (**Fig. 5a, b**). Additionally, we measured latency time to first entry to the dark chamber and found significantly higher latency time in PBS treated group whereas wildtype and cocktail treated groups showed similar latency time (**Fig. 5c**). Subsequently, we conducted longitudinal visual cliff test, a method employed to assess depth perception and the fear of crossing the deep side of a platform[36-38]. Typically, normal mice exhibit an inherent tendency to avoid the deep side, favoring instead the shallow side of a visual cliff. Mice were positioned on the central platform between the deep and shallow sides, and their choices were meticulously documented. Our observations revealed that wild-type mice displayed a notable preference, with 96±3.9% choices to shallow side. In contrast, the NMDA+PBS group exhibited a significantly diminished performance, with only 32±8.9% choosing the shallow side. Conversely, the cocktail-treated group demonstrated a more favorable outcome, with 72±10.9% of choices directed towards the shallow side (**Fig. 5d, e**). In assessing the cumulative duration of stay on both the shallow and deep sides, it became evident that wild-type mice exhibited a distinct preference towards the shallow side. Conversely, the NMDA+PBS group showed no clear preference, indicating a compromised performance. Intriguingly, the NMDA plus cocktail-treated mice displayed a preference for the shallow side (**Fig. 5f**). These findings strongly indicate a recovery of visual functions in NMDA injured cocktail-treated mice.

***In vitro* CiRGCs exhibits RGC like gene expression and chromatin signature.**

To reinforce our *in vivo* findings suggesting Müller glia is the source of endogenous RGC generation, we conducted experiment where human primary Müller and fibroblast cells were treated with similar chemical cocktail (VCRFIs+2F, without S24795) in a defined RGC differentiation medium (**Extended data Table 3, 4**). S24795 was omitted because *in vitro* Müller cells are already activated as indicated by their GFAP expression and may behave like progenitors[39]. Subsequently, we performed the RGC reprogramming and examined immunofluorescence with RGC markers on day 4. We observed that the morphology of CiRGCs resembled that of neurons, and these RGC-like cells exhibited

the expression of RBPMS, SNCG and BRN3A (**Extended data Fig. 5a-d)**. Müller derived RGC (*Md*-CiRGC) reprogramming was quick with *BRN3A* cells starting to appear as early as 6hrs after chemical induction (**Extended data Fig. 5e**). To achieve a deeper understanding of RGC gene expression we conducted SC-RNA Seq of CiRGCs collected on day 4 (**Fig. 6a)**. A total of 9044 *Md*-CiRGCs were included in the analysis and resulting data were visualized by UMAP and heatmap. We identified cell populations that are divided into 12 distinct clusters (**Fig. 6b**). These CiRGCs express all major RGC markers exhibited in heatmap and UMAP, including *BRN3A, RBPMS, ISL2, ISL1, SNCG, NEFL, NEFM, ELAVL3, ELAVL4,* as well as the RGC specifying transcription factor *SOX4* (**Fig. 6c, Extended data Fig. 6a, b)***.* Additionally, gene expression signature indicated the presence of mature RGC genes such as *THY1, GAP43, TUBB3* (**Extended data Fig. 6c)**. Reduced expression of Müller specific genes SLC1A3 (GLAST) and GFAP in the reprogrammed CiRGCs was noted (**Extended data Fig. 6d)**. We analyzed cell sets for POU4F1^{+} and POU4F1^{+}RBPMS^{+} (two best RGC markers across species) and examined expressions of major RGC genes. We found expressions of all major RGC specifying genes *SNCG, RBPMS, ISL2, ISL1, SNCG, NEFL, NEFM, ELAVL3, SOX4, THY1, TUBB3, GAP43* (**Fig. 6c. middle, lower**). Next, we examined if human fibroblasts can be reprogrammed to CiRGCs using same chemical method by SC-RNA seq. Fibroblast derived CiRGCs (*Fd*-CiRGCs) on day4 was used for single cell RNA sequencing similar to *Md*-CiRGCs. Notably, we found *Fd*-CiRGCs expressing RGC marker *BRN3A* along with other major RGC markers such as *BRN3B, RBPMS, SNCG, ISL2, NEFM, NEFL, GAP43, THY1, ISL1, ELAVL3, SOX4* etc. which is similar to *Md*-CiRGC gene expression signature (**Extended data Figs. 7a-c and 8)**. Neither Md nor *Fd* CiRGCs do not express other retinal cell markers (**Extended data Fig. 7d).**

Next, we examined the global chromatin signature of CiRGCs using SC-ATAC seq and t-SNE analysis indicated the existence of 8 major clusters based on a feature called promoter sum (**Fig. 6d**). Next promoter regions of all individual RGC genes were examined for presence of open chromatins using the filter function of the algorithm. BRN3A containing cells are distributed in all the clusters except one potentially immature cluster (#8) similar to our SC-RNA Seq (**Fig. 6d, e**). These BRN3A positive cells contain peaks or open chromatins in all the RGC promoters such as POU4F1, SNCG, NEFL,

ISL1, RBPMS, ISL2, NEFM, SOX4 (**Fig. 6f-h, Extended data Fig. 9**). Interestingly, no peaks were available in majority of cells at promoters of, SOX11, POU4F2 and GFAP which showed expression in few cells SC-RNA Seq (**Extended data Fig. 9d, e, h**). These results suggest that 6C+2F cocktail can reprogram human Müller cells and fibroblasts into CiRGCs.

SOX4 and NF-kB (RelA) collaboratively determine RGC fate from Müller cells.

We investigated mechanism behind CiRGC reprogramming from Müller cells using SC-RNASeq data. In this process, NF-kB emerged as a key player in the reprogramming of CiRGCs, based upon its established role in chemically mediated photoreceptor reprogramming from our prior study[27]. Photoreceptor reprogramming involved the use of VCRF which triggered the activation of NF-kB. Given the presence of VCRF in the CiRGC reprogramming cocktail, we hypothesized that NF-kB, either independently or in conjunction with other transcription factors, could directly regulate RGC fate determining genes such as *BRN3A, RBPMS, ISL1, SNCG and GAP43.* Previous report and our bioinformatics analysis (rVista) identified NF-kB binding sites in the regulatory regions of these genes (**Extended data Fig. 10**)[40]. Heatmap analysis of SC-RNA Seq indicated existence of an intermediate unstable progenitor-like stage representing clusters 1, 11 and 12 (**Extended data Fig. 11a, green box**). Approx. 30%-40% cells in these clusters express RGC specifying transcription factor SOX4, a potential target of WNT signaling activator CHIR9902 used in our cocktail[41]. In contrast, few cells in clusters 1, 11, 12 express NF-kB, compared to 30%-50% in the remaining clusters. These results suggested that SOX4$^+$ progenitors may have originated in clusters 1,11, 12 which subsequently express NF-kB and moved to other clusters. Further analysis revealed the existence of a few SOX4$^+$NF-kB$^+$ cells in clusters 1,11 and 12 and this number was increased in other clusters (**Extended data Fig. 11b, green box**). Trajectory analysis further confirmed that *SOX4$^+$NF-kB$^+$* cells originated in clusters 1, 11 and 12 subsequently spread to the rest of the clusters in later time points (**Extended data Fig. 11c, left)**. Investigating the potential induction of *BRN3A* expression, we examined the expression of *BRN3A* along with *SOX4$^+$NF-kB$^+$* cells. Interestingly, a few BRN3A-expressing cells were present in clusters 1,11,12, suggesting a gradual generation of *BRN3A$^+$* RGCs

(**Extended data Fig. 11c, middle**). A similar distribution was evident for *SOX4*$^{+}$*NF-kB*$^{+}$*POU4F1*+ cells (**Extended data Fig. 11c, right**). Trajectory analysis for all clusters along pseudotime indicated an initial origin of clusters 1 followed by clusters 5, 6, and then the remaining clusters, reinforcing the notion of a time-dependent generation of CiRGCs (**Extended data Fig. 11d**). Subsequently, we employed violin plots to illustrate gene expression patterns in *BRN3A*$^{+}$ and *BRN3A*$^{+}$*RELA*$^{+}$*SOX4*$^{+}$ cell sets (**Extended data Fig. 12**). Analysis of the *BRN3A*$^{+}$ cell population indicated that clusters 1 and 11 exhibited a few BRN3A^{+} cells, likely due to the presence of a limited number of *NF-kB*$^{+}$ or *SOX4*$^{+}$ cells (**Extended data Fig. 12a)**. In contrast, a higher number of *BRN3A*$^{+}$ cells were evident in the remaining clusters, where both *NF-kB* and SOX4 were co-expressed. Additionally, *BRN3A*$^{+}$*NF-kB*$^{+}$*SOX4*$^{+}$ population was revealed, clusters 1, 11, 12 do not possess these cells (**Extended data Fig. 12b)**. Collectively, these results further underscore the hypothesis that the cooperation between NF-kB and SOX4 contributes to BRN3A expression in CiRGCs similar to other studies where collaboration between SOX4 and RelA was noted[42] (**Extended data Fig. 12c)**. We also found *RAX*$^{+}$ progenitor like and *ATOH7*$^{+}$ cell population that may generate CiRGCs through a minor POU4F2 mediated pathway (**Extended data Fig. 11e**).

Discussion:

In our prior study we demonstrated the generation of photoreceptors from fibroblasts by 5C within 10 days. Since we observed cells morphologically similar to RGCs between reprogramming day 4 & 5 using 5C, we hypothesized that we might achieve the generation of RGCs at an earlier time point. Employing a Sncg promoter reporter our investigation indeed yielded GFP^{+} cells on day4, strongly indicating their RGC lineage (**Extended data Figs. 13 step1** & **14a**). Subsequently, we discovered PAX6^{+} (progenitor marker) cells on day 3, suggesting that 5C-mediated human retinal neuron reprogramming from fibroblasts may occur through a progenitor like stage (**Extended data Fig. 14b**)[43]. This was further supported by SC-RNA Seq showed presence of reminiscent PAX6^{+} cells on day 4 (**Extended data Fig. 14c**). Next, we investigated if 5C could reprogram human Müller cells into CiRGCs. Encouragingly, we observed the expression of Sncg-driven GFP in *Md*-CiRGCs, however when 5C coupled with 2F, we

noted a higher number of GFP$^+$ cells (**Extended data Figs. 13 step2, 14d-f**). These findings spurred us to investigate the potential of 5C+2F in regenerating RGCs from endogenous Müller cells. Administering this combination into NMDA-injured mice eye, we observed the proliferation of Müller cells, predominantly at the outer edge of the INL, albeit at reduced efficiency. A few were observed to progress towards GCL (**Extended data Fig. 15a**). At this stage, we searched for additional molecules that could potentially induce BrdU$^+$ Müller cell proliferation and facilitate their neurogenesis. We considered S24795, a partial agonist of α7 nAChR, given its established role in neural progenitor cell survival and CNS neurogenesis[44]. Finally, we found S24795 along with 5C+2F (but not S24795 alone) was able to enhance Müller cell proliferation and migration. Lineage tracing with a TdTomato reporter confirmed the Müller cell origin of regenerated CiRGCs, which extended their axons through the optic nerve head into the proximal part of optic nerve—a crucial step for visual function restoration. Consistently, we found recovery of visual functions starting from day 16, which reached its peak level on day 60. We noted differential vision improvement between right and left eyes on day 16 and day 23, with right eye improved better. This may be due to variability of RGC subtypes between left and right eyes which connect differentially with newly regenerated CiRGC axons[45]. Encouragingly, we generated CiRGCs from human primary Müller and fibroblasts by this chemical-only approach, offering its potential applications in humans. Interestingly, *Fd*-CiRGCs are immature (not expressing maturation marker *THY1*), hence would be ideal for cell transplantation. *Md*-CiRGCs express both vision-forming and pan RGC markers *BRN3A* and *RBPMS*, which are reported to be the best RGC markers across species[46-50]. Interestingly, *Md*-CiRGCs exhibited axon growth-enhancing genes (**Extended data Fig. 15b**) and 90% of BRN3A$^+$ *Md*-CiRGCs express the αRGC marker SPP1, a subtype, possess a greater propensity to regenerate their axons after axotomy[51, 52]. These results suggest a pro-regenerative state in CiRGCs, that support its regenerative ability in mice *in vivo* studies. Interestingly, αRGCs are most susceptible to injury in rat bead and ONC model and BRN3A$^+$ *Md*-CiRGCs isolated from *in vitro* culture would be ideal for transplantation studies in these models[53]. Furthermore, BRN3A$^+$ larger RGCs are preferentially susceptible to death in human glaucoma and BRN3A$^+$ endogenously regenerated *Md*-CiRGCs would be appropriate for therapy[54]. Our mechanistic study

suggests that NF-κB and SOX4 could have a central role in the formation of CiRGCs from primary Müller glia, representing a probable *in vivo* mechanism. We do not rule out the possibility for generation of certain CiRGCs through an ATOH7-dependent pathway, as we have identified a minor CiRGC population expressing ATOH7.

In summary, this study introduces a chemical-only strategy that effectively triggers endogenous RGC regeneration from Müller cells and rescue vision after RGC degeneration. This technique has the potential to overcome challenges associated with cell transplantations and could prove valuable in treating retinal neurodegenerative disorders such as glaucoma and optic nerve hypoplasia.

Acknowledgements. B.M. is supported by Knights Templar Eye Research Foundation, Glaucoma Research Foundation and Children's Hospital Los Angeles start up fund. We thank the stem cell analytics core, cellular imaging core, and special biology and genomics core at Children's Hospital Los Angels for pilot grant support and data collection. We thank Drs. David Cobrinik, Thomas Lee, Aaron Nagiel, Mark Borchert for critical review of the results.

Competing Interests. All other authors declare no competing interest. B.M. and R.M.S. are listed as inventors in a disclosure for patent application submitted to office of technology and commercialization at CHLA.

Author Contributions. B.M. designed experiments; B.M, wrote the manuscript; R.M.S, A, S, and BM: performed experiments.

Figure Legends:

Fig. 1. Small molecule cocktail (6C+2F) induces endogenous Müller cell proliferation, migration, and trans-differentiation to SNCG$^+$ RGCs post NMDA injury. (a) Scheme showing time point for small molecule cocktail intravitreal injections and subsequent tissue collection. (b) BrdU$^+$ cells in the lower part of INL layer 1 day after cocktail injection. (c, d) BrdU$^+$ cells are positive for Müller cell marker Glutamine Synthetase (GS). (e) BrdU$^+$ cells are migrated to GCL layer on day3 after injection. (f)

Number of $BrdU^+$ cells in the GCL layer on day3. (g) On day3, $BrdU^+$ cells in GCL layer are positive for RGC marker SNCG. (h) Number of $SNCG^+BrdU^+$ cells in the GCL layer.

Fig. 2. Lineage tracing using a AAV2-GLAST-GFP reporter confirms Müller origin of RGCs in NMDA injured retina. (a) Scheme showing time points for AAV2 and small molecule cocktail injection and subsequent tissue collections. (b) Upper panel: vehicle control. Middle panel: $BrdU^+$ cells are generated in the lower part of INL layer on day1 after cocktail injection and these $BrdU^+$ cells are GFP^+ (upper panel, inset white box). Lower panel: On day3 $BrdU^+$ GFP^+ cells (yellow) appeared in the GCL layer indicating their Müller origin. (c) GFP^+ cells in GCL layer are also positive for pan RGC marker RBPMS. (d) GFP^+ $BrdU^+$ cell count in the INL layer. (e, f) GFP^+ $BrdU^+$ and GFP^+RBPMS^+ cell counts in the GCL layer.

Fig. 3. CiRGC Lineage tracing and axon projection to the optic nerve in GLAST-Cre;Rosa26-TdTomato reporter mice. (a) Outline for the lineage tracing experiment. (b) Upper panel: Representative image showing $RBPMS^+$ $TdTomato^+$ cells (red and green rectangle) in the GCL layer on day3 indicating their Müller origin. (c) Magnified picture from red and green rectangular box. (d) No $TdTomato^+$ axons were evident in optic nerve of control eyes after NMDA and PBS treatment (n=3 eyes tested). $TdTomato^+$ cells are positive for muller specific marker GS. (e) Upper panel: WT control. Middle panel: PBS injected eyes showed no $TdTomato^+$ axon passing through the optic nerves on day6. Lower panel: In cocktail treated animals $TdTomato^+$ axons are passed through the optic nerve head on day 6. (f) Regenerated $TdTomato^+TUBB3^+$ axons passed through proximal part of optic nerve. (g) Magnified picture from (f) showing passed axons in the proximal part of optic nerve in cocktail treated eyes. (h) Magnified image for $TdTomato^+TUBB3^+$ axons passing through the optic nerve head into the proximal part of optic nerve.

Fig. 4. Recovery of pERG & pVEP after cocktail treatment in NMDA injured mice eye. (a) Timeline for functional measurements after cocktail treatment in NMDA injured eyes. (b) Recovery of pERG upon cocktail treatment. Upper panel: cocktail treated. Lower panel: PBS treated. Representative pERG waveforms are from day 23. (c) Pattern VEP

measurements at the indicated time points. Upper panel: cocktail treated. Lower panel: PBS treated. Representative pVEP waveforms from day 23 are presented. All measurements were conducted longitudinally at indicated time points.

Fig. 5. Rescue of light aversion & depth perception behavior after cocktail treatment in NMDA injured mice eye. (a) Schematic of the experimental set up for light aversion behavior test. (b) Plot of mean time (± SEM) spent in the dark chamber by the indicated experimental groups. (c) Plot of mean latency time (± SEM) required to first entry to the dark chamber by the indicated experimental groups. (d) Schematic of the experimental set up for death perception test (visual cliff test). (d) Plot for percent shallow side chooser. Five trials were performed for each animal. (f). Plot for cumulative duration spent in deep or shallow sides by the indicated experimental groups after removal of the cliff. Student's t-test was used to determine significance in b,c,e. 2-Way ANOVA was used to determine significance in f.

Fig. 6. Gene expression and chromatin analysis of *Md*-CiRGCs by SC-RNASeq and SC-ATAC Seq. (a) Scheme showing CiRGC generation from human primary Müller cells (HMC) and human lung fibroblasts (HFL). (b) UMAP analysis revealed 13 major clusters in Md-CiRGCs on day4 of reprogramming. (c) Heatmap analysis showing expression of all major RGC specifying genes (*Brn3a, Rbpms, Sncg, Isl2, Isl1, Sox4, Gap43, BIII-Tubulin, Thy1* etc) in total cell population, POU4F1^{+} and POU4F1^{+}RBPMS^{+} cell sets. (d) t-SNE analysis of SC-ATAC-Seq data using promoter sum function indicated presence of 8 total clusters. (e) Cells with open POU4F1 promoter peaks used for subsequent promoter analysis. (f-h) Open promoter peaks in the indicated genes.

Extended data Fig. 1. Generation of NMDA induced RGC degeneration mice model. (a) Retinal cross sections showing RBPMS^{+} cell death 7 days after NMDA injection in intravitreal route. (b) Approx. 72% decrease in RGC number was evident (n=3 eyes). (c) Retinal flat mount stained with RBPMS also showed decrease in RGC number. (d) Approx 80% decrease in RGC number was evident. RGCs were counted in periphery and medium regions (n=3 eyes).

Extended data Fig. 2. Generation of BrdU$^+$ cells is 6C+2F treated retina but not in vehicle treated retina. (a) Flat mount retina on day1 and day3 after BrdU antibody staining. (b) Magnified micrographs of flat mount retina showing BrdU staining in the DAPI$^+$ nucleus. (c) Retinal sections stained with BrdU in PBS injected eyes on day 1 and day 3, did not show any BrdU$^+$ cells. (d) No BrdU$^+$ cells were evident in PBS injected flat mount retina.

Extended data Fig. 3. AAV2-GLAST-GFP promoter reporter expression in Müller cells. (a) GFP expression from the reporter concentrated in the INL layer of the retina. (b) No GFP expression was evident in RBPMS$^+$ cells in GCL. (c) GFP reporter expressed in the nucleus of GS$^+$ Müller cells.

Extended data Fig. 4. Regenerated TdTomato$^+$ RGCs pass their axons through the optic nerve head and proximal part of the optic nerve. (a) No RBPMS+TdTomato+ cells were present in PBS injected retina on day3. (b) percentage of TdTomato$^+$RBPMS$^+$ cells in GCL on day3 after cocktail administration. (c) Mean fluorescence for TUBB3 staining (n=3 eyes every fifth section was counted) (d) Number of TdTomato$^+$ axons per section in the optic nerve. Every fifth section was counted from serial sections and 4 sections were included per eye (n=3). (e) TdTomato$^+$ axons pass through the optic nerve head in chemical treated eyes on day 6. (f) Z-section from the indicated area from d., showing axon passing through the optic nerve head (arrowheads). Black and white images are grayscaled and inverted.

Extended data Fig. 5. *In vitro* generation of CiRGCs from human primary Müller (*Md*-CiRGCs) and fibroblasts (*Fd*-CiRGCs). (a) RBPMS (green) and BRN3A (red) staining in *Md*-CiRGCs on day4. (b) qPCR showing increased expression of major RGC specifying genes in *Md*-CiRGCs on day4. (c) Left: *Fd*-CiRGCs express BRN3A in the nucleus (see white box). Right: SNCG-GFP promoter reporter expression in *Fd*-CiRGCs on day 4 (anti-GFP staining). (d) qPCR showing expression of major RGC genes in *Fd*-

RGCs (day4). (e). Time course expression measurement of *Brn3a* mRNA by qPCR in *Md*-CiRGCs.

Extended data Fig. 6. Visualizing expression of major RGC genes in *Md*-CiRGCs by UMAP analysis. (a-c) *Md*-CiRGCs are mostly *Brn3a* expressing RGCs and express other RGC marker genes [*Brn3b (few), Sncg, Isl2, Isl1, NefL, NefM, Elavl3*], specification genes (*Sox4*) and maturation genes such as (*Thy1, Gap43, Tubb3).* (d) Müller specific genes *Glast, Gfap* not expressed in most cells *Md*-CiRGC population indicating complete cell conversion. GFAP was expressed in 100% cells in the starting human Müller cells (immunofluorescence stydy, data not shown).

Extended data Fig. 7. Reprogramming human adult fibroblasts to Fd-CiRGCs by chemical cocktail and gene expression analysis by SC-RNASeq. (a-c) Heatmap analysis showing expression of all major RGC specifying genes (*Brn3a, Rbpms, Sncg, Isl2, Isl1, Sox4, Gap43, BIII-Tubulin, Thy1* etc.) in total CiRGC population, *Pou4f1*$^{+}$ and *Pou4f1*$^{+}$*Rbpms*$^{+}$ cell sets. (d) No or very few cells express photoreceptor specifying genes in *Pou4f1*$^{+}$ and *Pou4f1*$^{+}$ *Rbpms*$^{+}$ CiRGCs from both Müller cells and fibroblasts.

Extended data Fig. 8. visualizing major RGC genes in *Fd*-CiRGCs by UMAP analysis (a) UMAP analysis of *Fd*-CiRGCs revealed 9 major clusters on day4 of reprogramming. (b, c) *Fd*-CiRGCs are mostly POU4F1 and POU4F2 expressing. FdCiRGCs express RGC marker genes (*Rbpms, Sncg, Isl1, Isl2, NefL, NefM*), specifying genes (*Sox4*) and maturation genes (*Tubb3, Gap43, Thy1*). (d) Fibroblasts specific genes *NefH, Col1a2* not expressed in *Fd*-CiRGCs, indicating complete cell conversion.

Extended data Fig. 9. Open promoter peaks present in the indicated RGC specifying genes in POU4F1 promoter sum+ cells. (a-g) Chromatin opening in promoters of the indicated genes. (h) GFAP have no open promoter peak.

Extended data Fig. 10. Bioinformatic analysis (r-vista) of NF-kB (RELA) binding site identification. Putative RelA binding sites are present in POU4F1, ISL1 regulatory regions.

Extended data Fig.11. SOX4 and NF-kB (RELA) mediates *Md*-CiRGC fate commitment through a non-canonical pathway. (a) *Md*-CiRGC SC-RNASeq showed presence of an unstable progenitor population that express *Sox4* but not *RelA* (upper panel, green and red boxes). This cell population was absent from *Pou4f1*$^+$ cell set (lower panel). (b) Few *RelA*$^+$*Sox4*$^+$ cells generated in cluster1, 11, 12 (UMAP, green boxes). However, numbers increased in the rest of the clusters. Left UMAP: all cell populations; middle UMAP: *RelA*$^+$*Sox4*$^+$ cells in different clusters, right UMAP; merged. (c) *RelA*$^+$*Sox4*$^+$ and *Pou4f1*$^+$ cells followed similar pattern of cluster wise distribution. Left UMAP: Pseudo time trajectory analysis of *RelA*$^+$*Sox4*$^+$ cells showing increased numbers in later time points at clusters other than 1, 11 and 12. Middle UMAP: Few *Sox4*$^+$*RelA*$^+$ and *Pou4f1*$^+$ cells were evident in clusters 1, 11 and 12. Right UMAP: Almost no *Sox4*$^+$*RelA*$^+$*Pou4f1*$^+$ cells were evident in clusters, 1, 11 and 12. (d) Pseudo time trajectory analysis (UMAP) for all clusters indicated clusters 1, 11, 12 generated earlier than other clusters where *Pou4f1* expressed. (e) Presence of *Rax*+ and *Atoh7*+ cells in CiRGC population on day4 (UMAP).

Extended data Fig. 12. SOX4 and NF-kB (RELA) mediates *Md*-CiRGC fate commitment through a non-canonical pathway. (a,b) Expression analysis of *RelA, Sox4 and Pou4f1* (violin plot) in Pou4f1$^+$ and Pou4f1$^+$Sox4$^+$RelA$^+$ cell sets. (c) Schematic diagram for the mechanism of CiRGC generation.

Extended data Fig. 13. Stepwise identification of small molecule cocktail for endogenous CiRGC regeneration. Step1: Scheme for stepwise generation of potential CiRGCs and progenitors by modifying 5C medicated photoreceptor generation protocol. Step2: Scheme for the generation of potential CiRGCs from human Muller cells using 5C plus 2 additional factors (2F, Noggin and IGF1). Step3: Scheme for identification of novel chemical cocktail for the generation of CiRGCs from Muller cells *in vivo*.

Extended data Fig. 14. Generation of CiRGCs from human primary Müller cells (HPM) and foreskin fibroblasts (HFF) on day4 and identification of PAX6+ progenitor cells in earlier time points (a) SNCG-GFP expressing CiRGCs from HADF on day4 of 5C-chemical reprogramming. (b) $PAX6^+$ and RAX^+ cells generated from HADF after day3 of 5C-reprogramming. (c) Reminiscent *Pax6*+ cells in SC-RNA-Seq after 6C+2F treatment in HADF on day4. (d) SNCG-GFP expressing CiRGCs from HPM on day4 of 5C-chemical reprogramming. (e) $PAX6^+$ and RAX^+ cells generated from HPM after day3 of 5C-reprogramming. (f) Reminiscent *Pax6*+ cells in SC-RNA-Seq after 6C+2F treatment in HPM on day4.

Extended data Fig. 15. (a) 5C+2F induces generation of $BrdU^+$ cells but with lower efficiency. (b) Expression of indicated axon regeneration genes in *Md*-CiRGCs.

References:

1. Tanaka, E.M. & Ferretti, P. Considering the evolution of regeneration in the central nervous system. *Nat Rev Neurosci* **10**, 713-723 (2009).
2. Li, H. & Chen, G. In Vivo Reprogramming for CNS Repair: Regenerating Neurons from Endogenous Glial Cells. *Neuron* **91**, 728-738 (2016).
3. Ming, G.L. & Song, H. Adult neurogenesis in the mammalian brain: significant answers and significant questions. *Neuron* **70**, 687-702 (2011).
4. Goldman, D. Müller glia cell reprogramming and retina regeneration *Nature Review Neuroscience* **15**, 431-442 (2014).
5. Jorstad, N.L. et al. Stimulation of functional neuronal regeneration from Muller glia in adult mice. *Nature* (2017).
6. Ueki, Y. et al. Transgenic expression of the proneural transcription factor Ascl1 in Muller glia stimulates retinal regeneration in young mice. *Proc Natl Acad Sci U S A* **112**, 13717-13722 (2015).
7. Cope, E.C. & Gould, E. Adult Neurogenesis, Glia, and the Extracellular Matrix. *Cell Stem Cell* **24**, 690-705 (2019).
8. He, G.Y.a.Z. Glial inhibition of CNS axon regeneration. *Nature Reviews Neuroscience* **7**, 617 (2006).
9. Goldman, S.A. Stem and Progenitor Cell-Based Therapy of the Central Nervous System: Hopes, Hype, and Wishful Thinking. *Cell Stem Cell* **18**, 174-188 (2016).

10. Trounson, A. & McDonald, C. Stem Cell Therapies in Clinical Trials: Progress and Challenges. *Cell Stem Cell* **17**, 11-22 (2015).
11. Kikuchi, T. et al. Human iPS cell-derived dopaminergic neurons function in a primate Parkinson's disease model. *Nature* **548**, 592-596 (2017).
12. Vierbuchen, T. et al. Direct conversion of fibroblasts to functional neurons by defined factors. *Nature* **463**, 1035-1041 (2010).
13. Victor, M.B. et al. Generation of human striatal neurons by microRNA-dependent direct conversion of fibroblasts. *Neuron* **84**, 311-323 (2014).
14. Xue, Y. et al. Direct conversion of fibroblasts to neurons by reprogramming PTB-regulated microRNA circuits. *Cell* **152**, 82-96 (2013).
15. Yoo, A.S. et al. MicroRNA-mediated conversion of human fibroblasts to neurons. *Nature* **476**, 228-231 (2011).
16. Liu, Y. et al. Ascl1 Converts Dorsal Midbrain Astrocytes into Functional Neurons In Vivo. *J Neurosci* **35**, 9336-9355 (2015).
17. Weinberg, M.S., Criswell, H.E., Powell, S.K., Bhatt, A.P. & McCown, T.J. Viral Vector Reprogramming of Adult Resident Striatal Oligodendrocytes into Functional Neurons. *Mol Ther* **25**, 928-934 (2017).
18. Niu, W. et al. SOX2 reprograms resident astrocytes into neural progenitors in the adult brain. *Stem Cell Reports* **4**, 780-794 (2015).
19. Gaia Colasante, G.L., Alicia Rubio, Lucian Medrihan, Latefa Yekhlef,Alessandro Sessa,Luca Massimino, Serena G. Giannelli, Silvio Sacchetti, Massimiliano Caiazzo, Damiana Leo, Dimitra Alexopoulou, Maria Teresa Dell'Anno, Ernesto Ciabatti, Marta Orlando, Michele Studer, Andreas Dahl, & Raul R. Gainetdinov, S.T., Fabio Benfenati, and Vania Broccoli Rapid Conversion of Fibroblasts into Functional Forebrain GABAergic Interneurons by Direct Genetic Reprogramming. *Cell Stem cell* **17**, 719-134 (2015).
20. ia Rivetti di Val Cervo, R.A.R., Giada Spigolon, Débora Masini, Elisa Martín-Montañe, Enrique M Toledo, Gioele La Manno, Michael Feyder, Christian Pifl2, Yi-Han Ng, Sara Padrell Sánchez, Sten Linnarsson, Marius Wernig, Tibor Harkany, Gilberto Fisone & Ernest Arenas induction of functional dopamine neurons from human astrocytes in vitro and mouse astrocytes in a Parkinson's disease model. *Nature Biotechnology* **35** (2017).
21. Torper, O. et al. In Vivo Reprogramming of Striatal NG2 Glia into Functional Neurons that Integrate into Local Host Circuitry. *Cell Rep* **12**, 474-481 (2015).
22. Guo, Z. et al. In vivo direct reprogramming of reactive glial cells into functional neurons after brain injury and in an Alzheimer's disease model. *Cell Stem Cell* **14**, 188-202 (2014).
23. Hu, W. et al. Direct Conversion of Normal and Alzheimer's Disease Human Fibroblasts into Neuronal Cells by Small Molecules. *Cell Stem Cell* **17**, 204-212 (2015).
24. Li, X. et al. Small-Molecule-Driven Direct Reprogramming of Mouse Fibroblasts into Functional Neurons. *Cell Stem Cell* **17**, 195-203 (2015).
25. Babos, K. & Ichida, J.K. Small Molecules Take a Big Step by Converting Fibroblasts into Neurons. *Cell Stem Cell* **17**, 127-129 (2015).
26. Zhang, L. et al. Small Molecules Efficiently Reprogram Human Astroglial Cells into Functional Neurons. *Cell Stem Cell* **17**, 735-747 (2015).
27. Mahato, B. et al. Pharmacologic fibroblast reprogramming into photoreceptors restores vision. *Nature* **581**, 83-88 (2020).

28. Takeda, M. et al. alpha-Aminoadipate induces progenitor cell properties of Muller glia in adult mice. *Invest Ophthalmol Vis Sci* **49**, 1142-1150 (2008).
29. Mike O. Karl, S.H., Branden R. Nelson, Kristine Tan, Brian Buckingham, and Thomas A. Reh Stimulation of neural regeneration in the mouse retina. *PNAS* **105**, 19508–19513 (2008).
30. Natalia Surzenko, T.C., Amelia Bachleda, Lee Langer and Larysa Pevny SOX2 maintains the quiescent progenitor cell state of postnatal retinal Müller glia. *Development* **140**, 1445-1455 (2013).
31. Shen, F. et al. Glutamate-induced glutamine synthetase expression in retinal Muller cells after short-term ocular hypertension in the rat. *Invest Ophthalmol Vis Sci* **45**, 3107-3112 (2004).
32. Miesfeld, J.B. et al. The Atoh7 remote enhancer provides transcriptional robustness during retinal ganglion cell development. *Proc Natl Acad Sci U S A* **117**, 21690-21700 (2020).
33. Bin Lin, A.K., Nobushige Tanaka, Satchidananda Panda, and Richard H. Masland Restoration of visual function in retinal degeneration mice by ectopic expression of melanopsin. *PNAS* **105**, 16009–16014 (2008).
34. Katada, Y. et al. Highly sensitive visual restoration and protection via ectopic expression of chimeric rhodopsin in mice. *iScience* **26**, 107716 (2023).
35. Divya, M.S. et al. Intraocular Injection of ES Cell-Derived Neural Progenitors Improve Visual Function in Retinal Ganglion Cell-Depleted Mouse Models. *Front Cell Neurosci* **11**, 295 (2017).
36. Gu, L., Kawaguchi, R., Caprioli, J. & Piri, N. The effect of Rbfox2 modulation on retinal transcriptome and visual function. *Sci Rep* **10**, 19683 (2020).
37. Guo, X. et al. Preservation of vision after CaMKII-mediated protection of retinal ganglion cells. *Cell* **184**, 4299-4314 e4212 (2021).
38. Su, J. et al. In vivo base editing rescues photoreceptors in a mouse model of retinitis pigmentosa. *Mol Ther Nucleic Acids* **31**, 596-609 (2023).
39. de Melo, J. et al. Injury-independent induction of reactive gliosis in retina by loss of function of the LIM homeodomain transcription factor Lhx2. *Proc Natl Acad Sci U S A* **109**, 4657-4662 (2012).
40. Takae Kiyama, H.Y.A., Tudor C. Badea, and Chai-An Mao. Pou4f1-Tbr1 transcriptional cascade controls the formation of Jam2-expressing retinal ganglion cells. *Frontiers in Ophthalmology* (2023).
41. Moreno, C.S. SOX4: The unappreciated oncogene. *Semin Cancer Biol* **67**, 57-64 (2020).
42. Jones, K. et al. SOX4 and RELA Function as Transcriptional Partners to Regulate the Expression of TNF- Responsive Genes in Fibroblast-Like Synoviocytes. *Front Immunol* **13**, 789349 (2022).
43. Till Marquardt, R.A.-P., Nicole Andrejewski, Raffaella Scardigli, Francois Guillemot, and Peter Gruss Pax6 Is Required for the Multipotent State of Retinal Progenitor Cells. *Cell* **105**, 43-55 (2005).
44. Kita, Y. et al. Galantamine promotes adult hippocampal neurogenesis via M(1) muscarinic and alpha7 nicotinic receptors in mice. *Int J Neuropsychopharmacol* **17**, 1957-1968 (2014).
45. Rheaume, B.A. et al. Single cell transcriptome profiling of retinal ganglion cells identifies cellular subtypes. *Nat Commun* **9**, 2759 (2018).

46. Francisco M. Nadal-Nicola´s, M.J.n.-L.p., Paloma Sobrado-Calvo, Leticia Nieto-Lo´pez, Isabel Ca´novas-Martínez, Manuel Salinas-Navarro, Manuel Vidal-Sanz, and Marta Agudo Brn3a as a Marker of Retinal Ganglion Cells: Qualitative and Quantitative Time Course Studies in Naïve and Optic Nerve–Injured Retinas. *Investigative Ophthalmology & Visual Science* **50**, 3860-3838-3868 (2009).
47. Iain M Dykes, J.L., S Raisa Eng, Eric E Turner Brn3a regulates neuronal subtype specification in the trigeminal ganglion by promoting Runx expression during sensory differentiation. *Neural Development* **5** (2010).
48. Quina, L.A. et al. Brn3a-expressing retinal ganglion cells project specifically to thalamocortical and collicular visual pathways. *J Neurosci* **25**, 11595-11604 (2005).
49. Vladimir Vladimirovich Muzyka, M.B.a.T.C.B. Postnatal developmental dynamics of cell type specification genes in Brn3a/Pou4f1 Retinal Ganglion Cells. *Neural Development* **13:15** (2018).
50. Nadal-Nicolas, F.M. et al. Pan-retinal ganglion cell markers in mice, rats, and rhesus macaques. *Zool Res* **44**, 226-248 (2023).
51. Gallego-Ortega, A. et al. Alpha retinal ganglion cells in pigmented mice retina: number and distribution. *Frontiers in Neuroanatomy*.
52. Duan, X. et al. Subtype-specific regeneration of retinal ganglion cells following axotomy: effects of osteopontin and mTOR signaling. *Neuron* **85**, 1244-1256 (2015).
53. VanderWall, K.B. et al. Differential susceptibility of retinal ganglion cell subtypes in acute and chronic models of injury and disease. *Sci Rep* **10**, 17359 (2020).
54. Lisa A. Kerrigan–Baumrind, H.A.Q., Mary E. Pease, Danielle F. Kerrigan, and Rebecca S. Mitchell Number of Ganglion Cells in Glaucoma Eyes Compared with Threshold Visual Field Tests in the Same Persons. *Invest Ophthalmol Vis Sci.* **41**, 741-748 (2000).

Fig.1

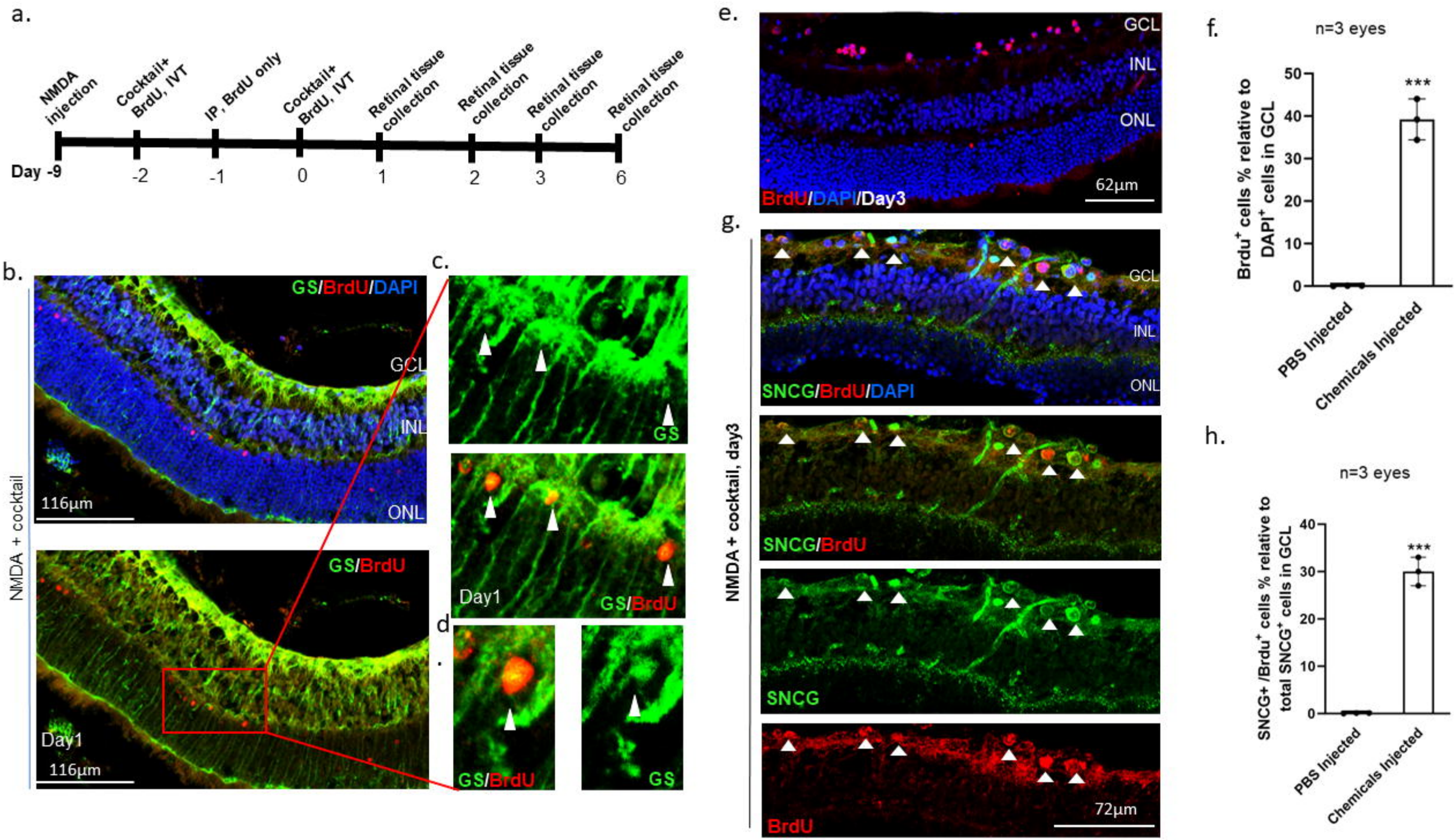
a.
NMDA injection
Cocktail+ BrdU, IVT
IP, BrdU only
Cocktail+ BrdU, IVT
Retinal tissue collection
Retinal tissue collection
Retinal tissue collection
Retinal tissue collection
Day -9
-2
-1
0
1
2
3
6
b.
GS/BrdU/DAPI
GCL
INL
ONL
116µm
GS/BrdU
Day1
116µm
NMDA + cocktail
c.
GS
Day1
GS/BrdU
d.
GS/BrdU
GS
e.
GCL
INL
ONL
BrdU/DAPI/Day3
62µm
g.
GCL
INL
ONL
SNCG/BrdU/DAPI
SNCG/BrdU
SNCG
BrdU
72µm
NMDA + cocktail, day3
f.
n=3 eyes
Brdu+ cells % relative to DAPI+ cells in GCL
50
40
30
20
10
0
***
PBS Injected
Chemicals Injected
h.
n=3 eyes
SNCG+ /Brdu+ cells % relative to total SNCG+ cells in GCL
40
30
20
10
0
***
PBS Injected
Chemicals Injected

Fig.2

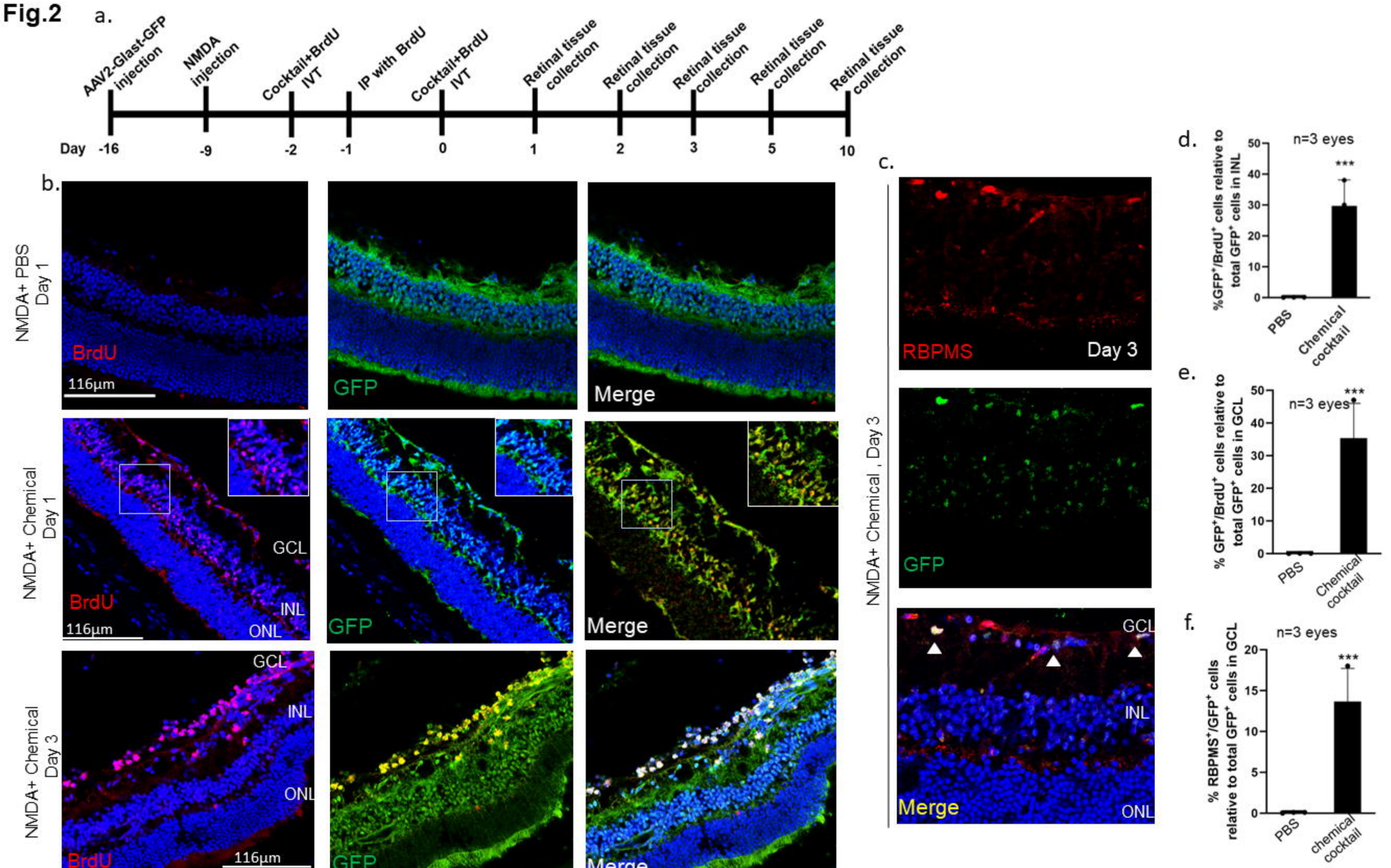
a.
AAV2-Glast-GFP injection
NMDA injection
Cocktail+BrdU IVT
IP with BrdU
Cocktail+BrdU IVT
Retinal tissue collection
Retinal tissue collection
Retinal tissue collection
Retinal tissue collection
Retinal tissue collection
Day -16
-9
-2
-1
0
1
2
3
5
10
b.
NMDA+ PBS Day 1
NMDA+ Chemical Day 1
NMDA+ Chemical Day 3
BrdU
GFP
Merge
116µm
GCL
INL
ONL
c.
NMDA+ Chemical , Day 3
RBPMS
Day 3
GFP
Merge
GCL
INL
ONL
d.
n=3 eyes
***
%GFP+/BrdU+ cells relative to total GFP+ cells in INL
PBS
Chemical cocktail
e.
n=3 eyes
***
% GFP+/BrdU+ cells relative to total GFP+ cells in GCL
PBS
Chemical cocktail
f.
n=3 eyes
***
% RBPMS+/GFP+ cells relative to total GFP+ cells in GCL
PBS
chemical cocktail

Fig.3

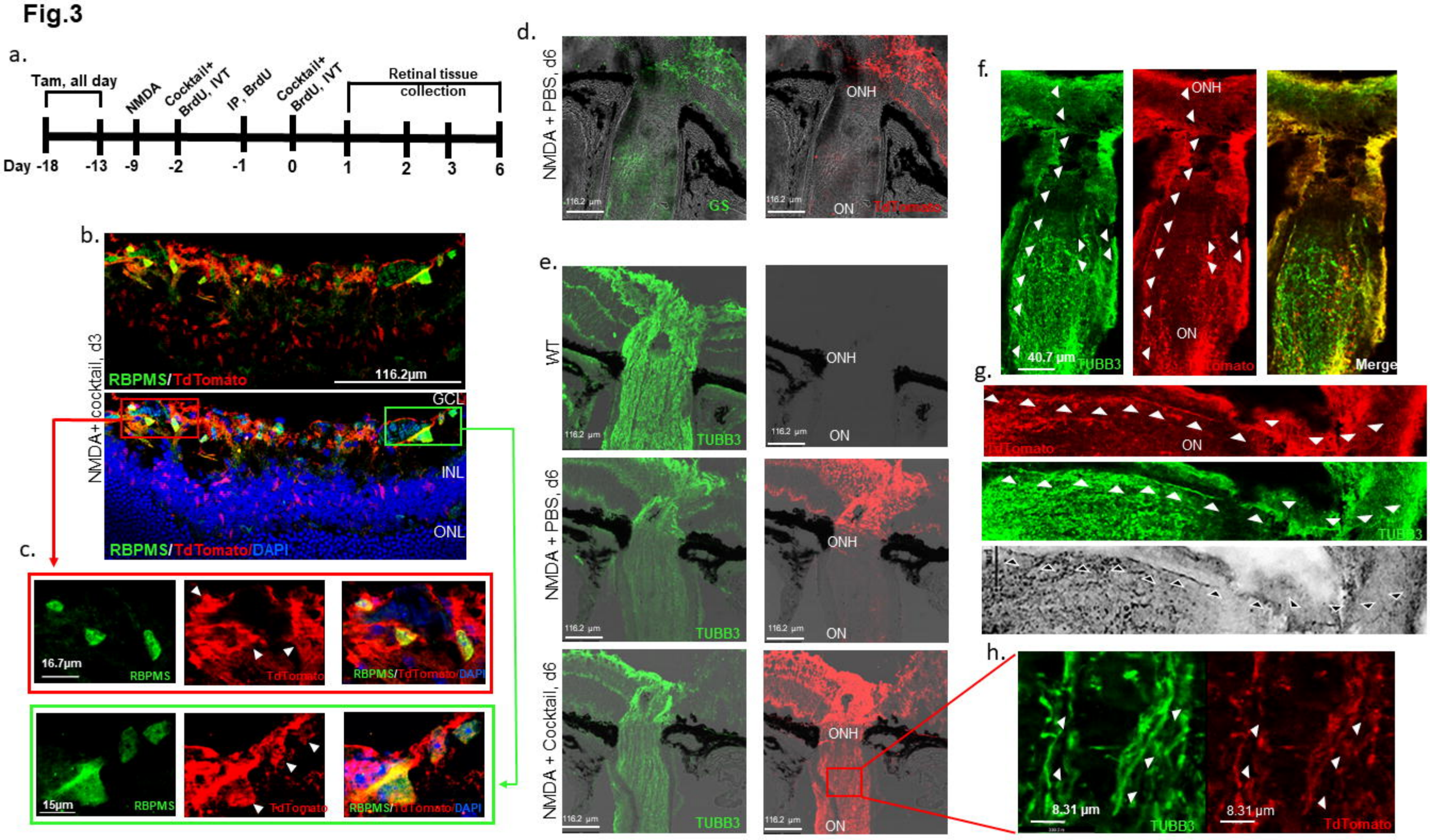
a.
Tam, all day
NMDA
Cocktail+ BrdU, IVT
IP, BrdU
Cocktail+ BrdU, IVT
Retinal tissue collection
Day -18
-13
-9
-2
-1
0
1
2
3
6
b.
NMDA+ cocktail, d3
RBPMS/TdTomato
116.2μm
GCL
INL
ONL
RBPMS/TdTomato/DAPI
c.
16.7μm
RBPMS
TdTomato
RBPMS/TdTomato/DAPI
15μm
RBPMS
TdTomato
RBPMS/TdTomato/DAPI
d.
NMDA + PBS, d6
116.2 μm
GS
ONH
ON
TdTomato
e.
WT
TUBB3
ONH
ON
NMDA + PBS, d6
NMDA + Cocktail, d6
f.
40.7 μm
TUBB3
ONH
ON
TdTomato
Merge
g.
TdTomato
ON
TUBB3
h.
8.31 μm
TUBB3
8.31 μm
TdTomato

Fig.4

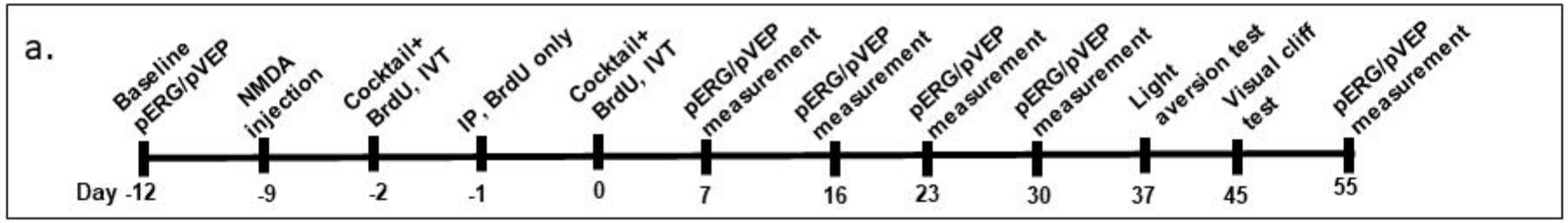
a.
Baseline pERG/pVEP
NMDA injection
Cocktail+ BrdU, IVT
IP, BrdU only
Cocktail+ BrdU, IVT
pERG/pVEP measurement
pERG/pVEP measurement
pERG/pVEP measurement
pERG/pVEP measurement
Light aversion test
Visual cliff test
pERG/pVEP measurement
Day -12
-9
-2
-1
0
7
16
23
30
37
45
55

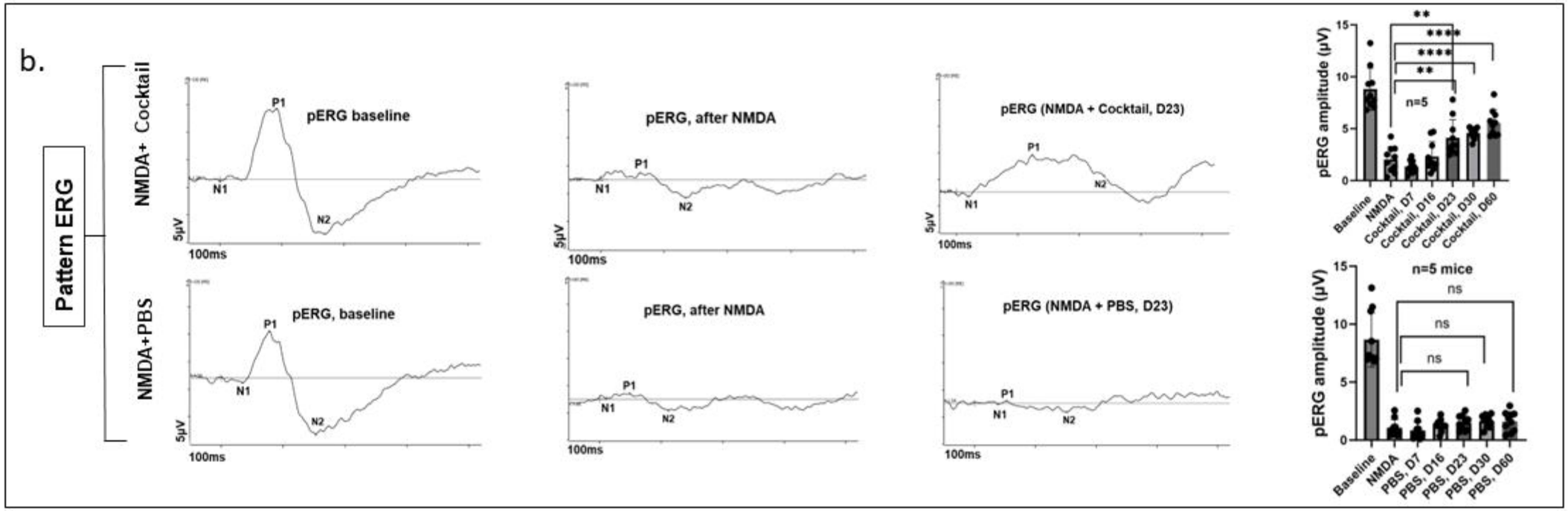
b.
Pattern ERG
NMDA+ Cocktail
NMDA+PBS
pERG baseline
pERG, after NMDA
pERG (NMDA + Cocktail, D23)
pERG, baseline
pERG, after NMDA
pERG (NMDA + PBS, D23)
P1
N1
N2
5μV
100ms
pERG amplitude (μV)
n=5
Baseline
NMDA
Cocktail, D7
Cocktail, D16
Cocktail, D23
Cocktail, D30
Cocktail, D60
n=5 mice
ns
PBS, D7
PBS, D16
PBS, D23
PBS, D30
PBS, D60

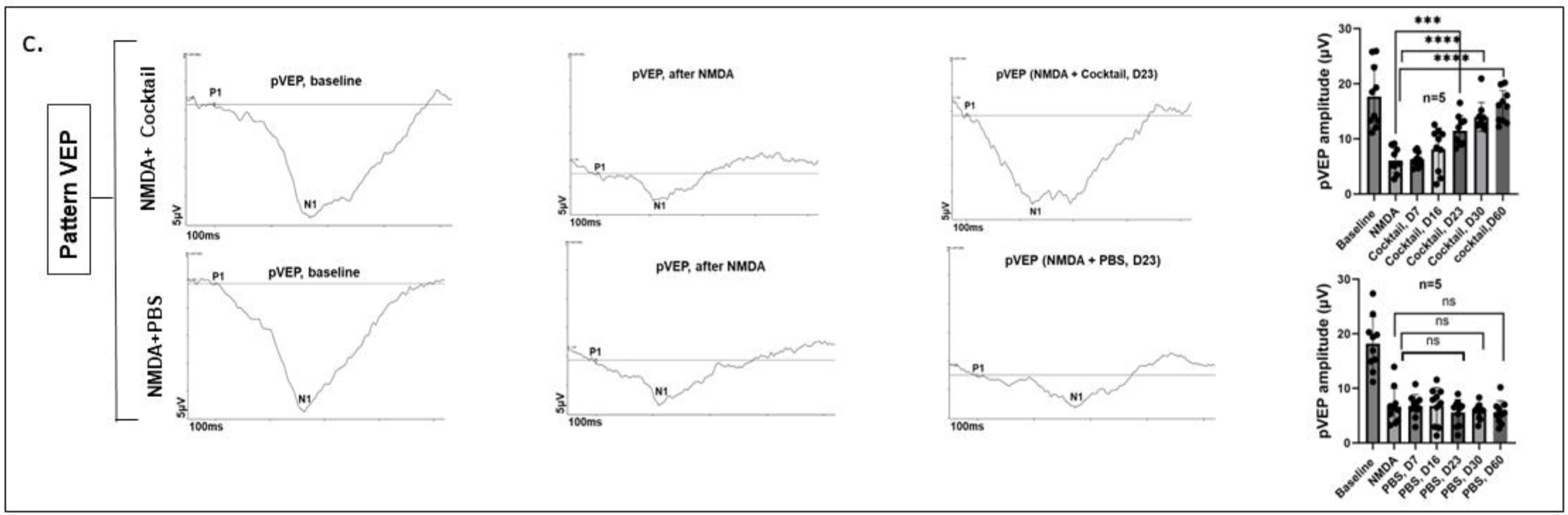
C.
Pattern VEP
NMDA+ Cocktail
NMDA+PBS
pVEP, baseline
pVEP, after NMDA
pVEP (NMDA + Cocktail, D23)
pVEP, baseline
pVEP, after NMDA
pVEP (NMDA + PBS, D23)
P1
N1
5μV
100ms
pVEP amplitude (μV)
n=5
Baseline
NMDA
Cocktail, D7
Cocktail, D16
Cocktail, D23
Cocktail, D30
cocktail,D60
ns
PBS, D7
PBS, D16
PBS, D23
PBS, D30
PBS, D60

Fig.5

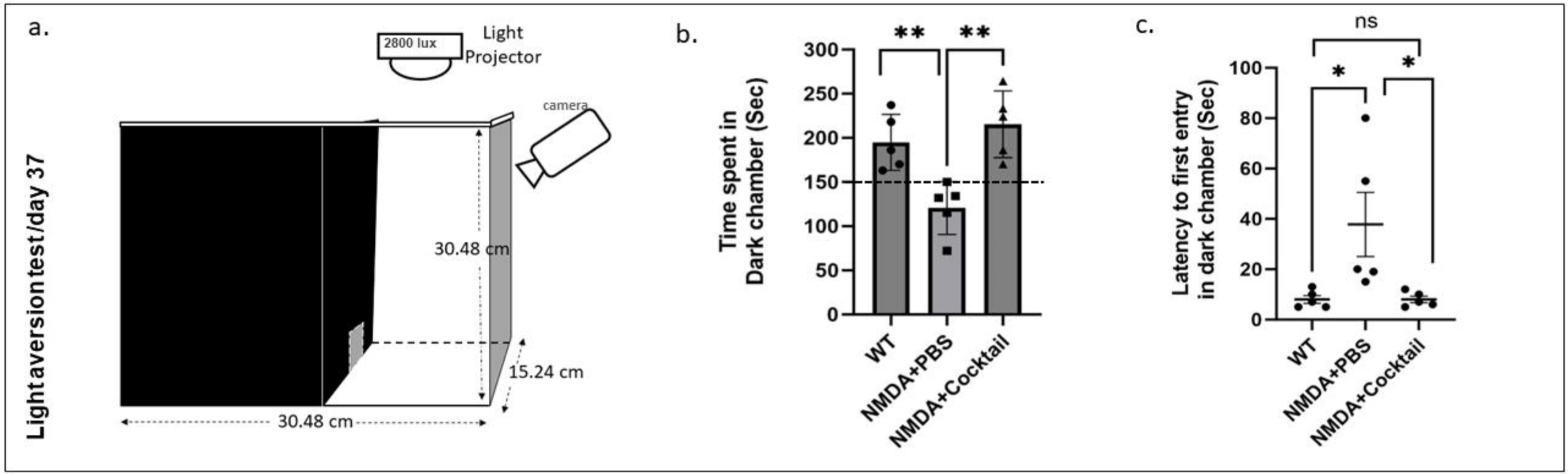
a.
Light aversion test/day 37
2800 lux
Light Projector
camera
30.48 cm
15.24 cm
30.48 cm
b.
Time spent in Dark chamber (Sec)
300
250
200
150
100
50
0
**
**
WT
NMDA+PBS
NMDA+Cocktail
c.
Latency to first entry in dark chamber (Sec)
100
80
60
40
20
0
ns
*
*
WT
NMDA+PBS
NMDA+Cocktail

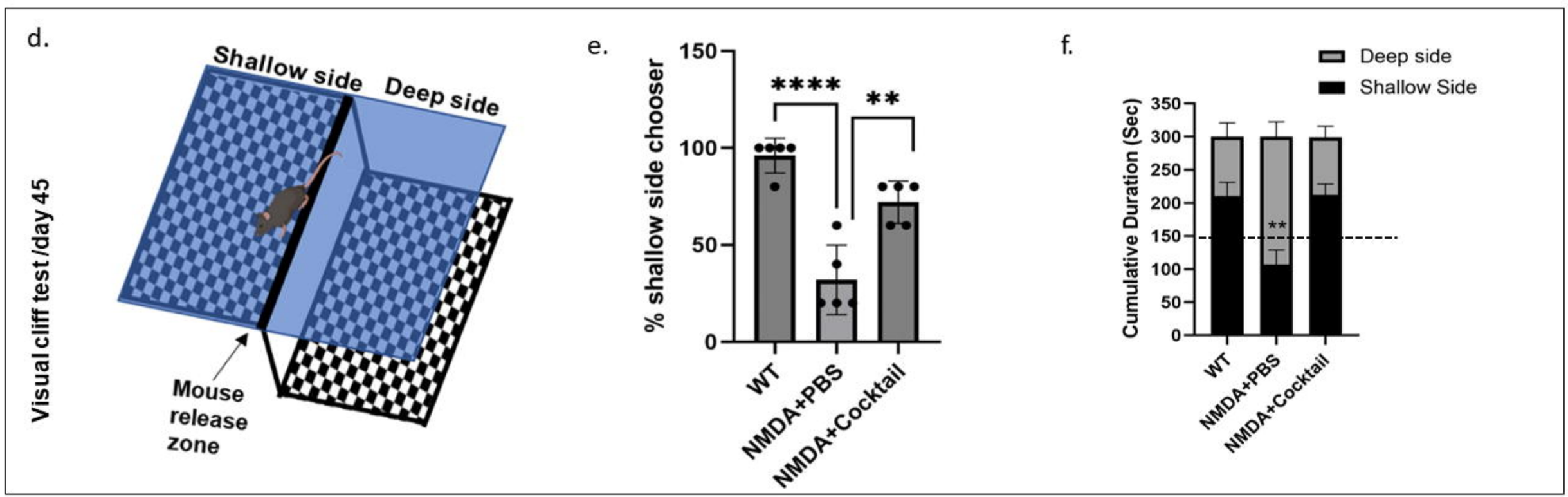
d.
Visual cliff test /day 45
Shallow side
Deep side
Mouse release zone
e.
% shallow side chooser
150
100
50
0
****
**
WT
NMDA+PBS
NMDA+Cocktail
f.
Deep side
Shallow Side
Cumulative Duration (Sec)
350
300
250
200
150
100
50
0
**
WT
NMDA+PBS
NMDA+Cocktail

Fig. 6

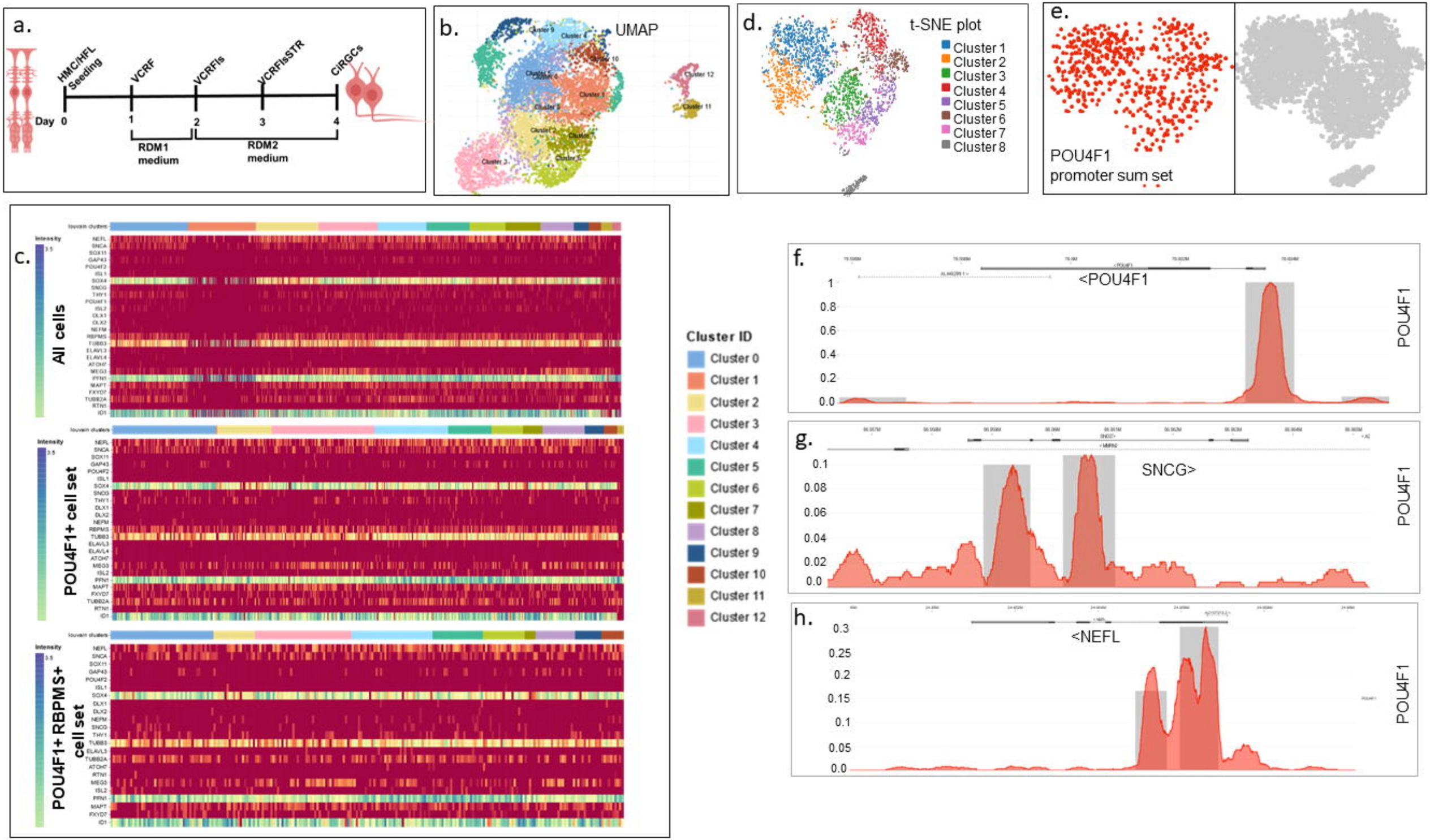
a.
HMC/HFL Seeding
VCRF
VCRFIs
VCRFIsSTR
CiRGCs
Day 0
1
2
3
4
RDM1 medium
RDM2 medium
b.
UMAP
d.
t-SNE plot
Cluster 1
Cluster 2
Cluster 3
Cluster 4
Cluster 5
Cluster 6
Cluster 7
Cluster 8
e.
POU4F1 promoter sum set
c.
All cells
POU4F1+ cell set
POU4F1+ RBPMS+ cell set
Cluster ID
Cluster 0
Cluster 1
Cluster 2
Cluster 3
Cluster 4
Cluster 5
Cluster 6
Cluster 7
Cluster 8
Cluster 9
Cluster 10
Cluster 11
Cluster 12
f.
<POU4F1
POU4F1
g.
SNCG>
POU4F1
h.
<NEFL
POU4F1

Extended data Fig.1

a.

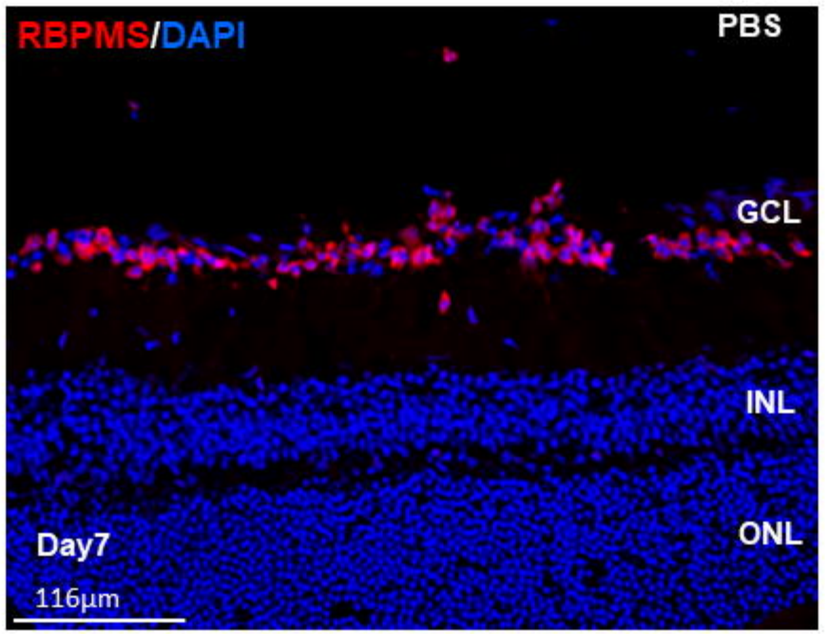

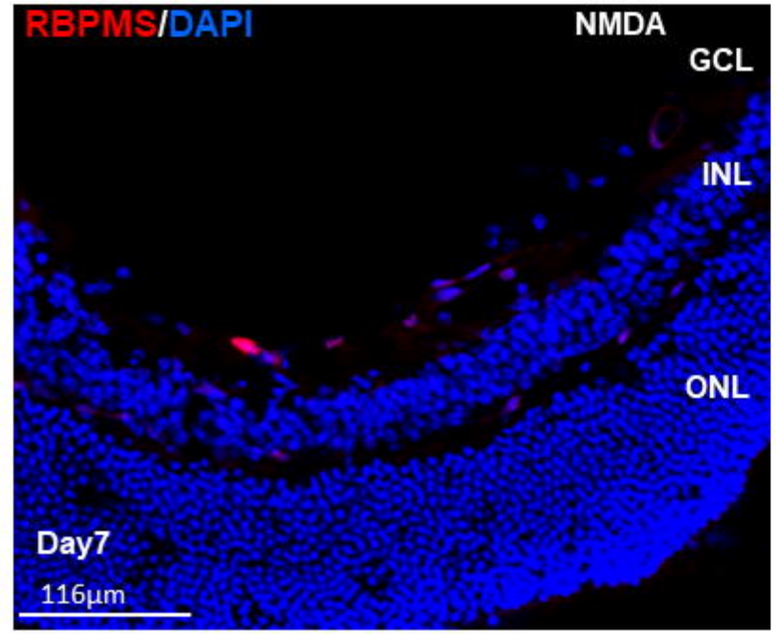

b.

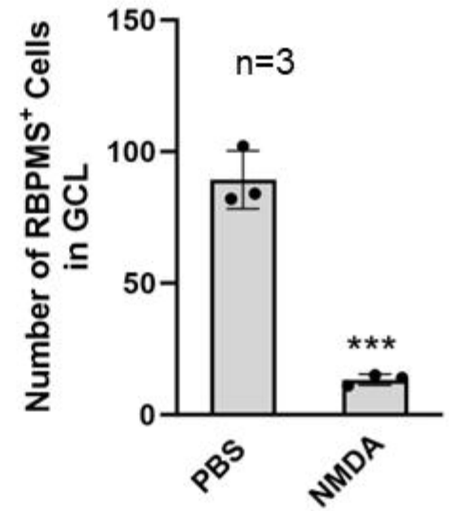

c.

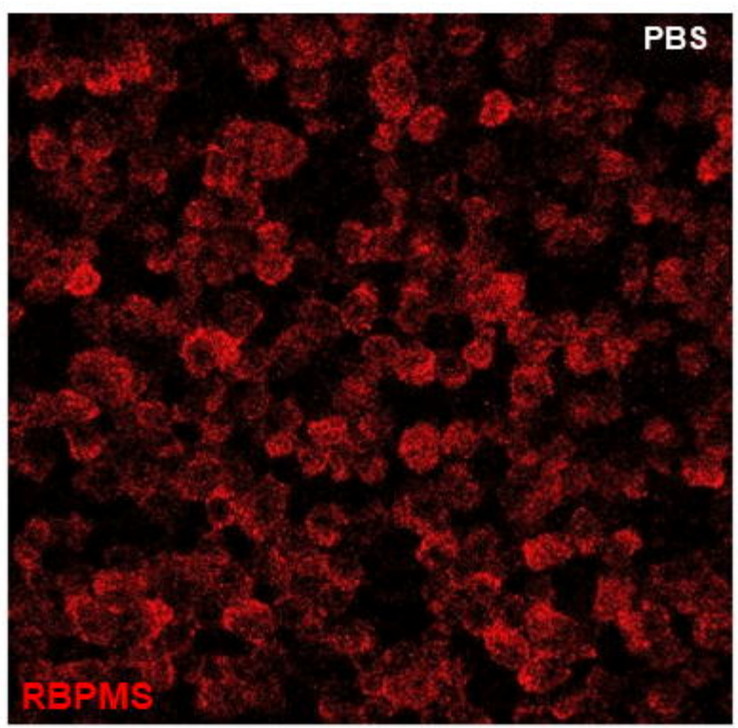

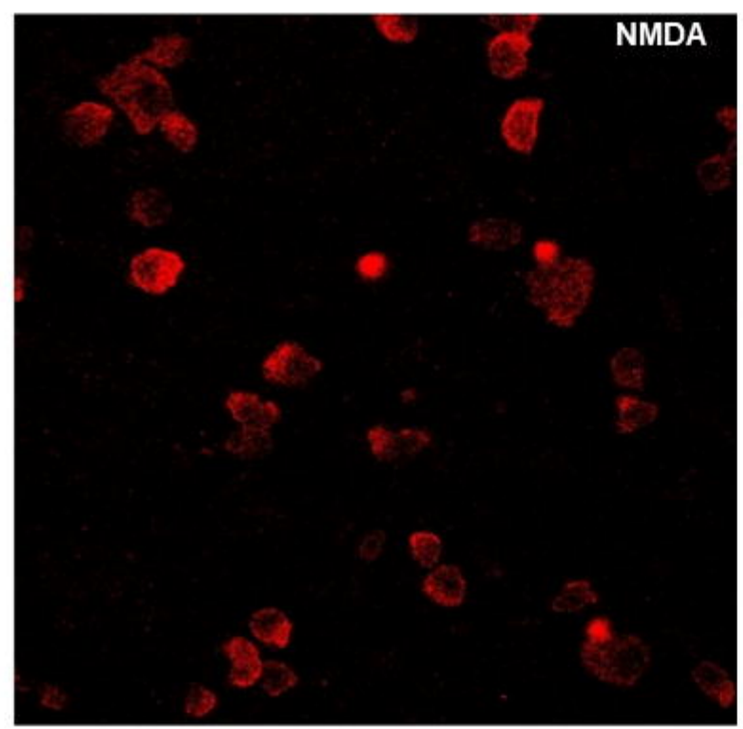

d.

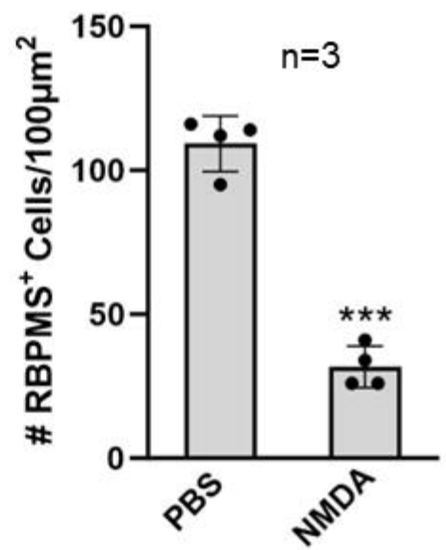

Extended data Fig.2

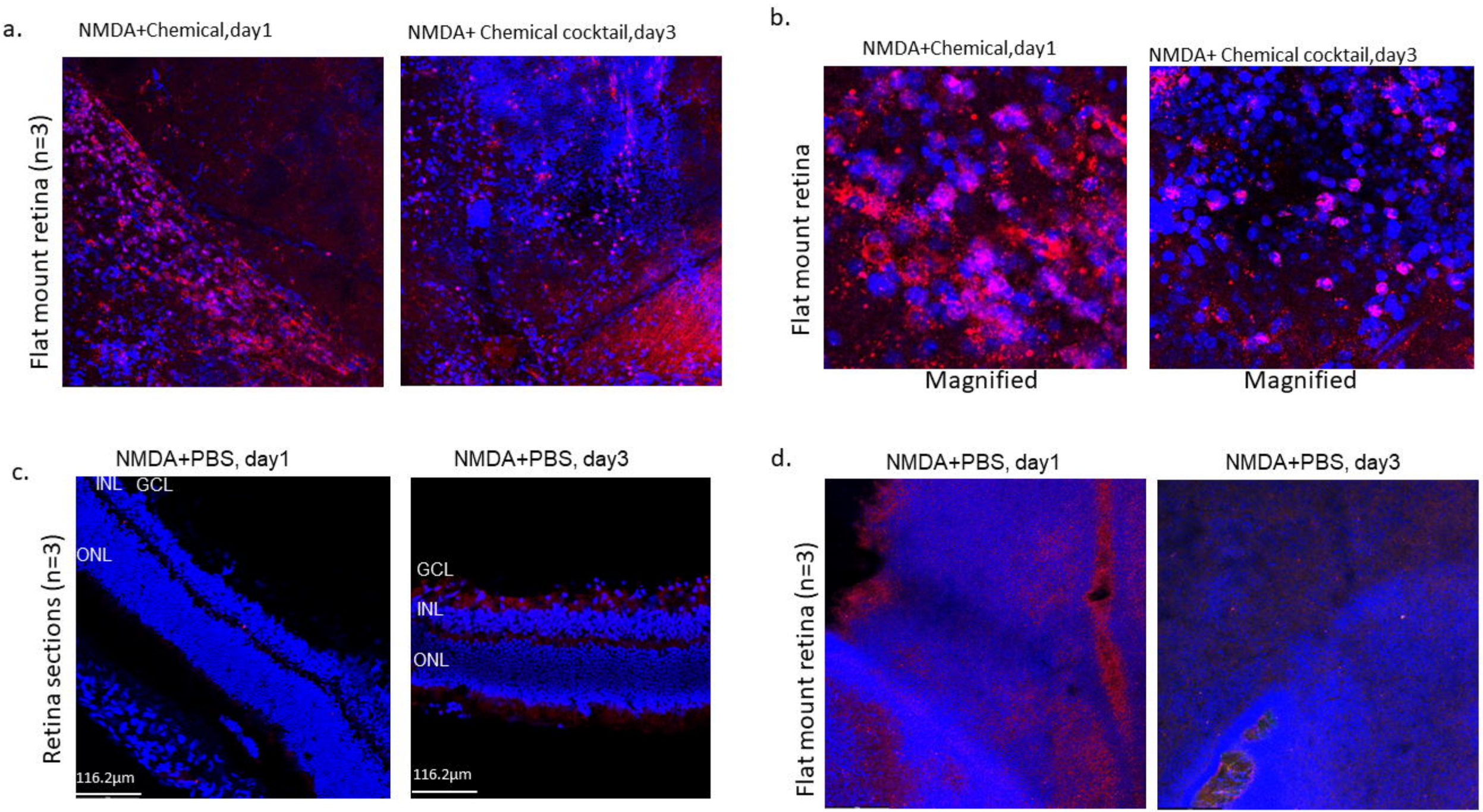

Extended data Fig.3

a.

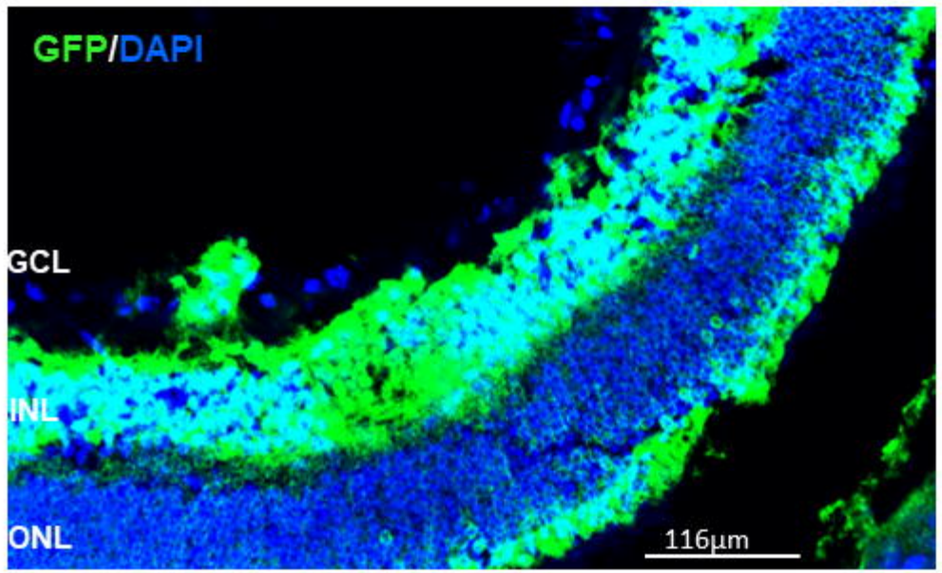

b.

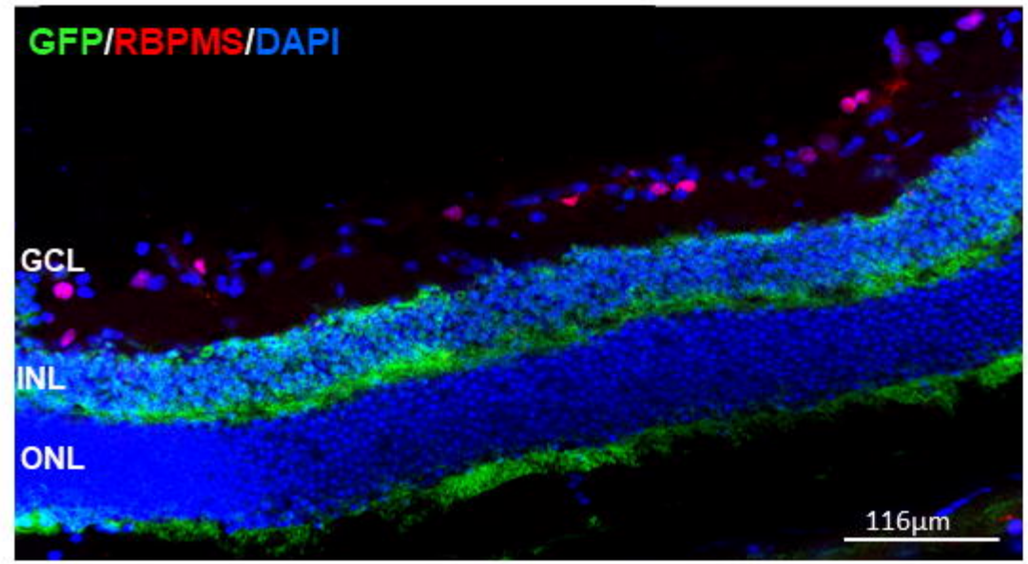

c.

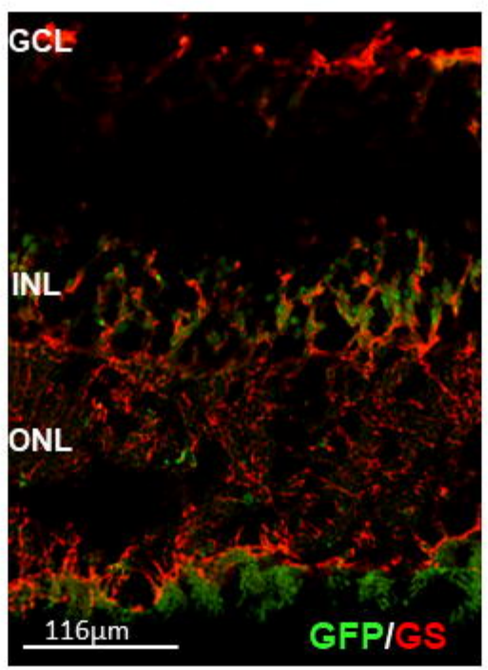

Extended data Fig.4

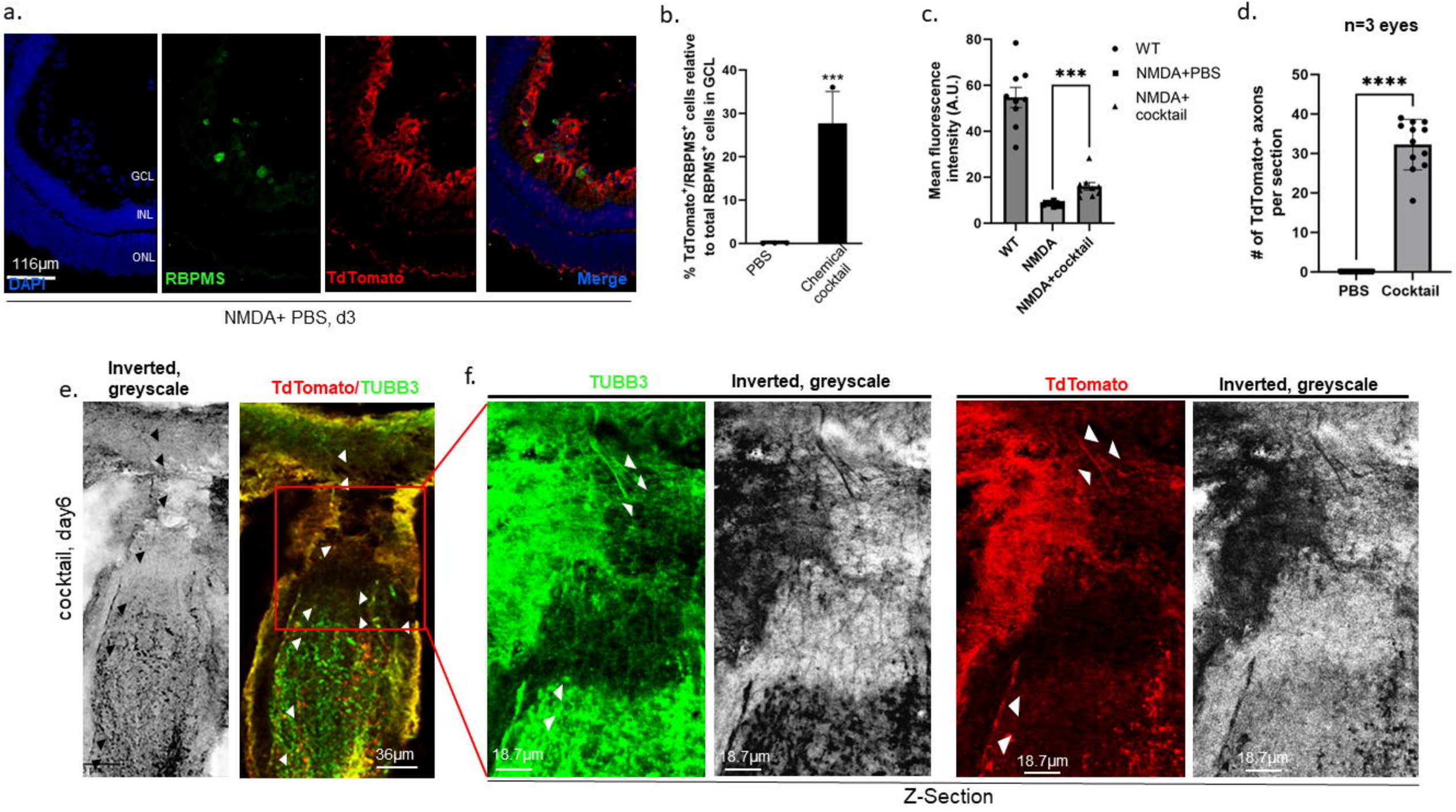

Extended data Fig.5

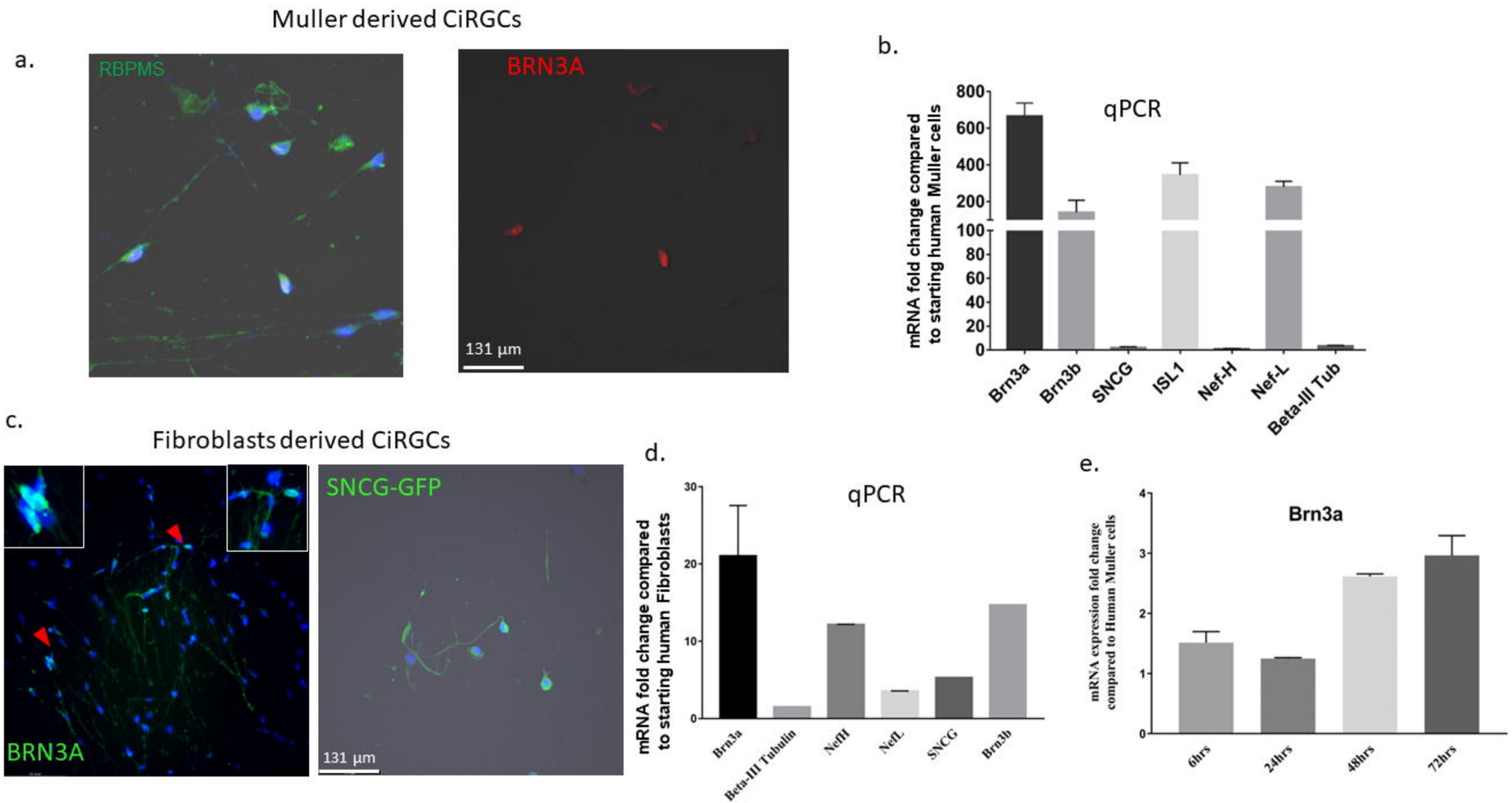

Extended data Fig.6

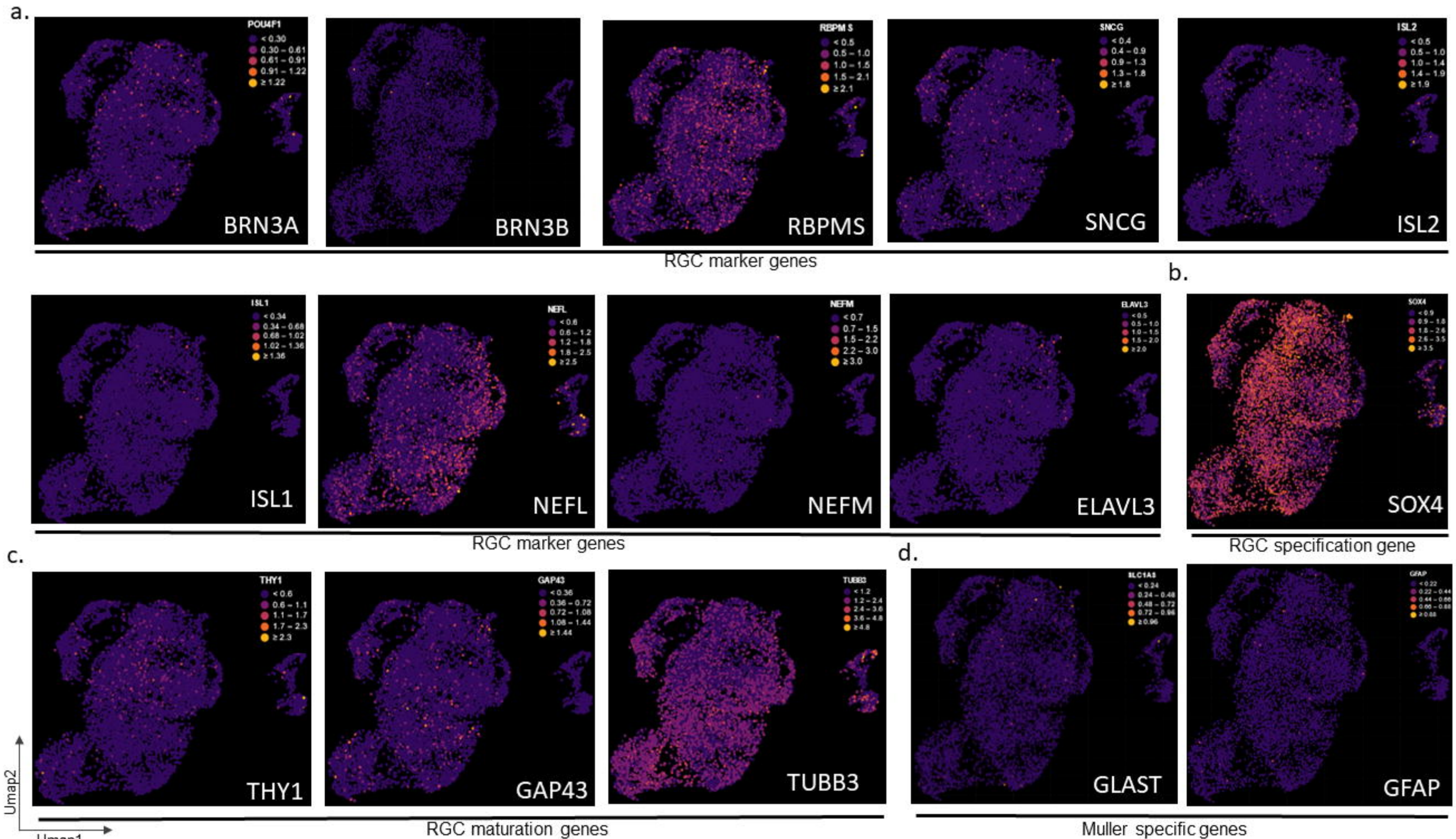

Extended data Fig.7

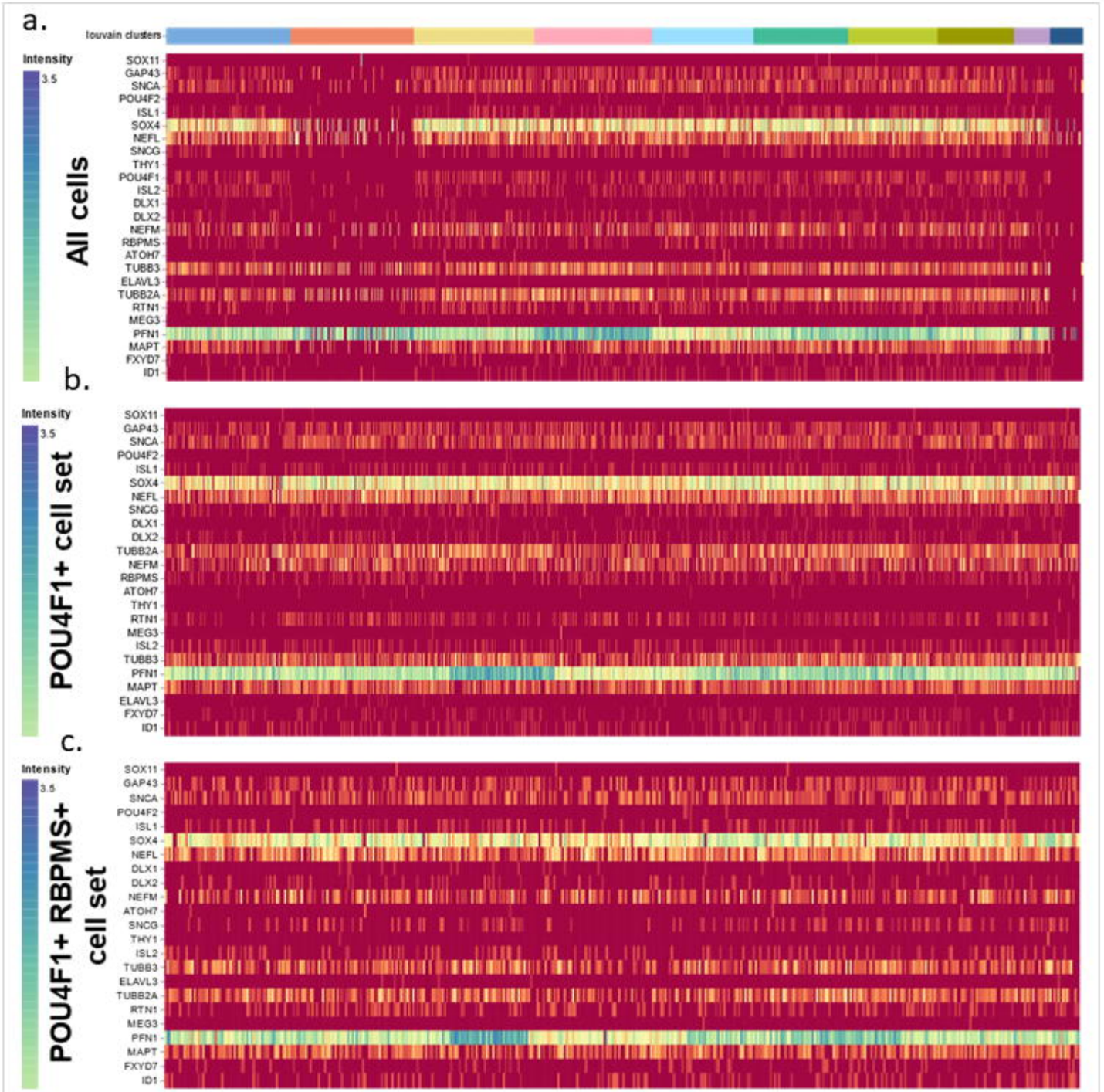

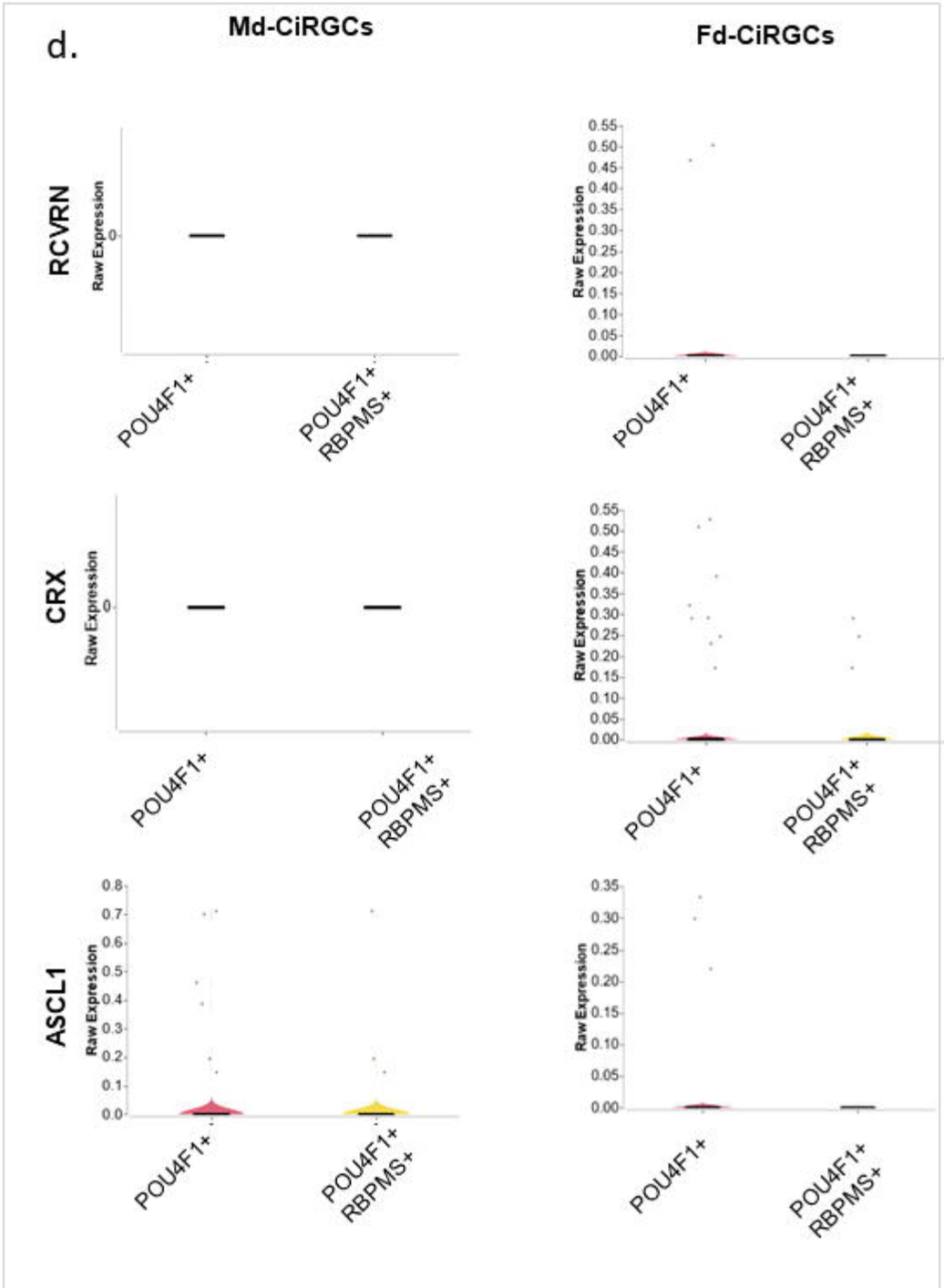

Extended data Fig.8

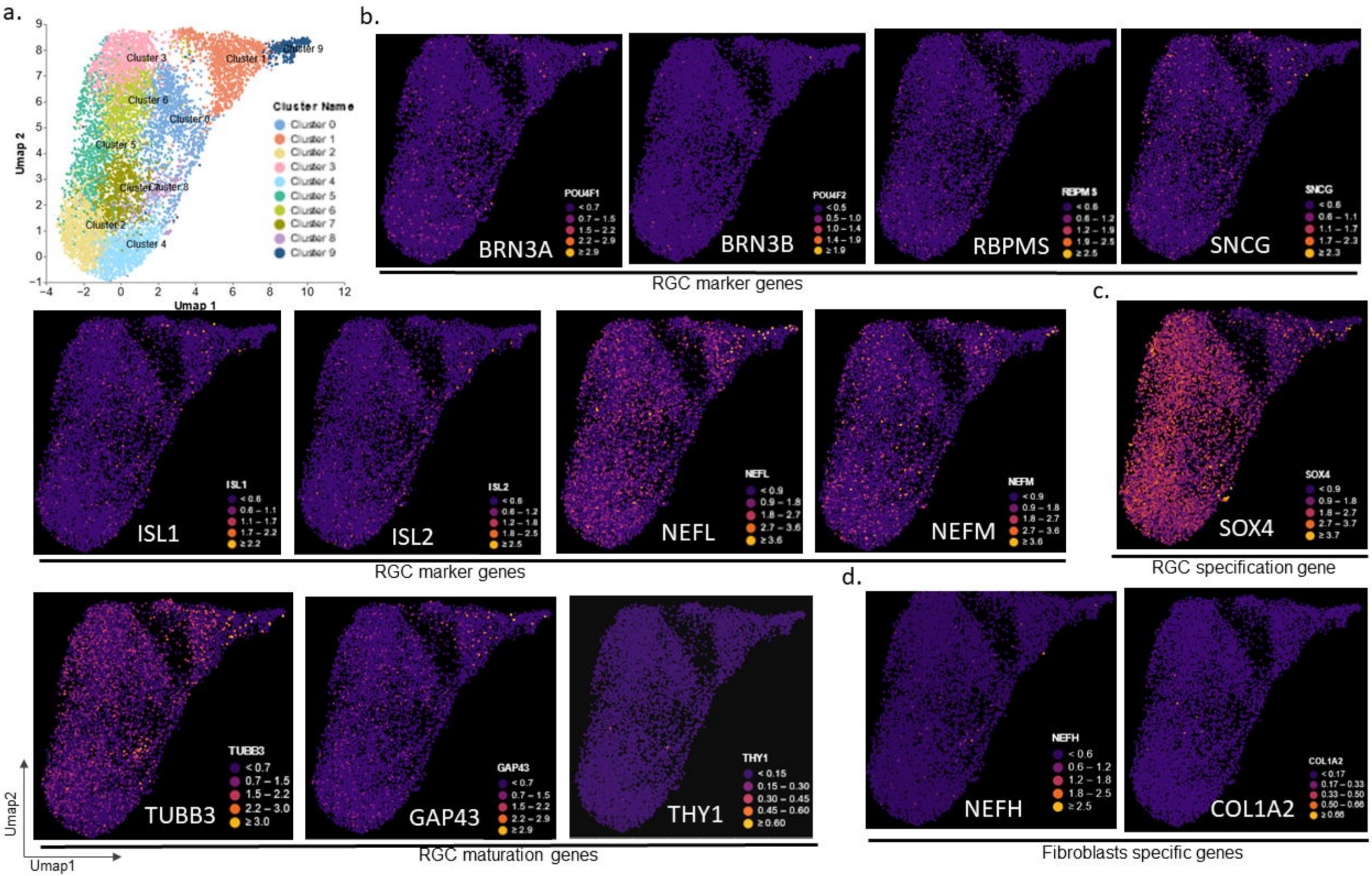

Extended data Fig.9

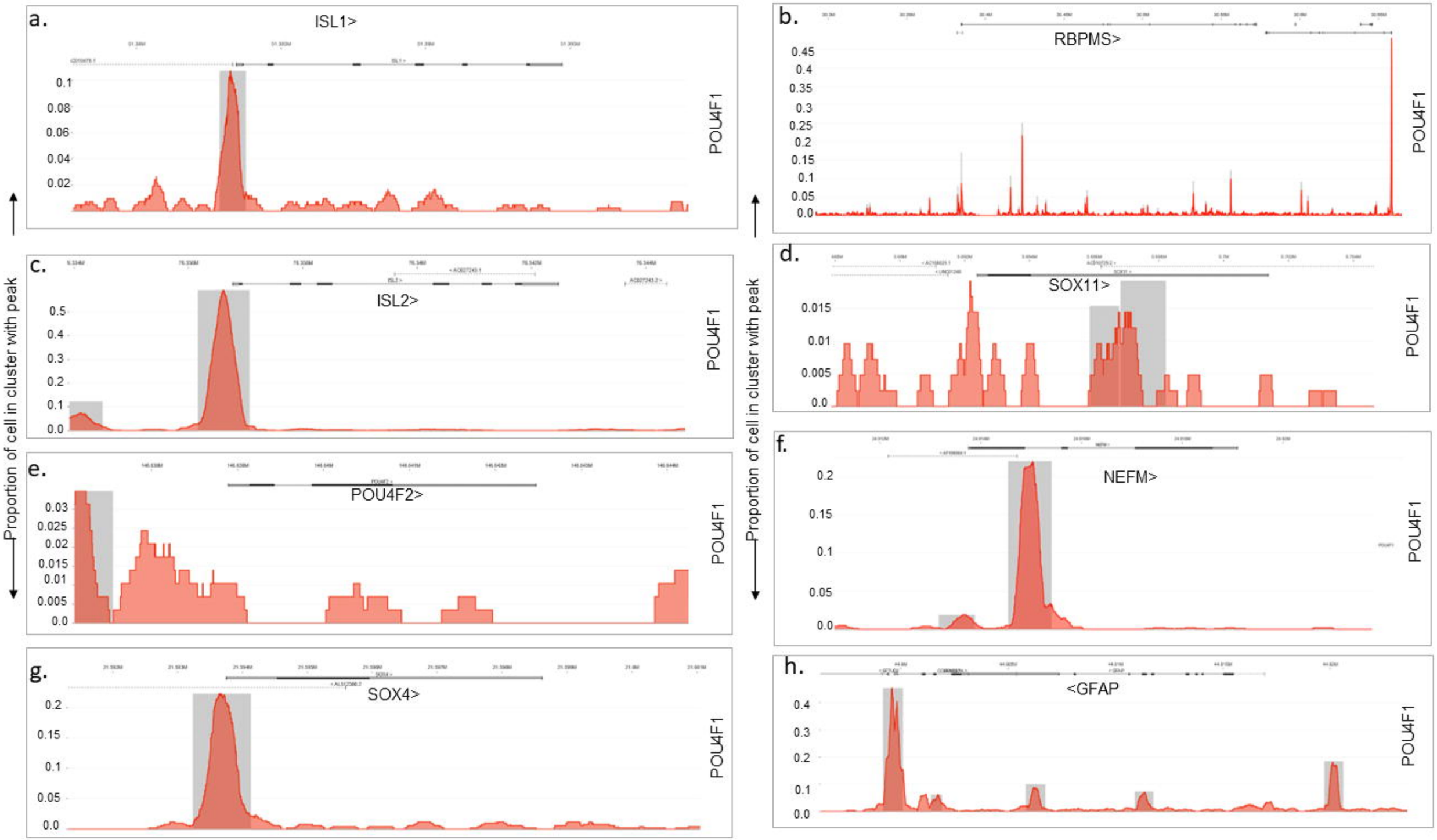

Extended data Fig.10

rVista analysis showing NF-kB binding sites in BRN3A, ISL1 genes

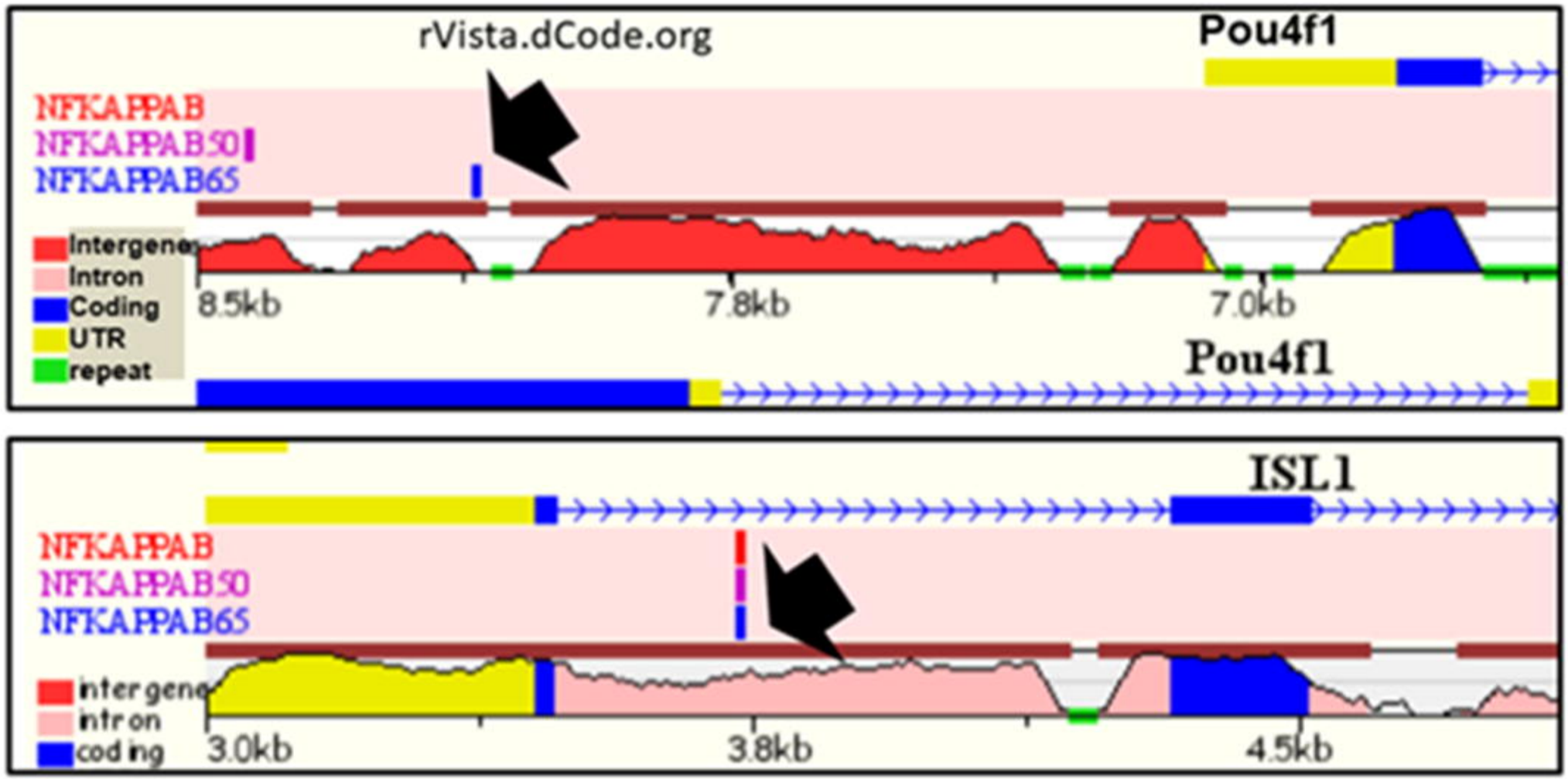

Extended data Fig.11

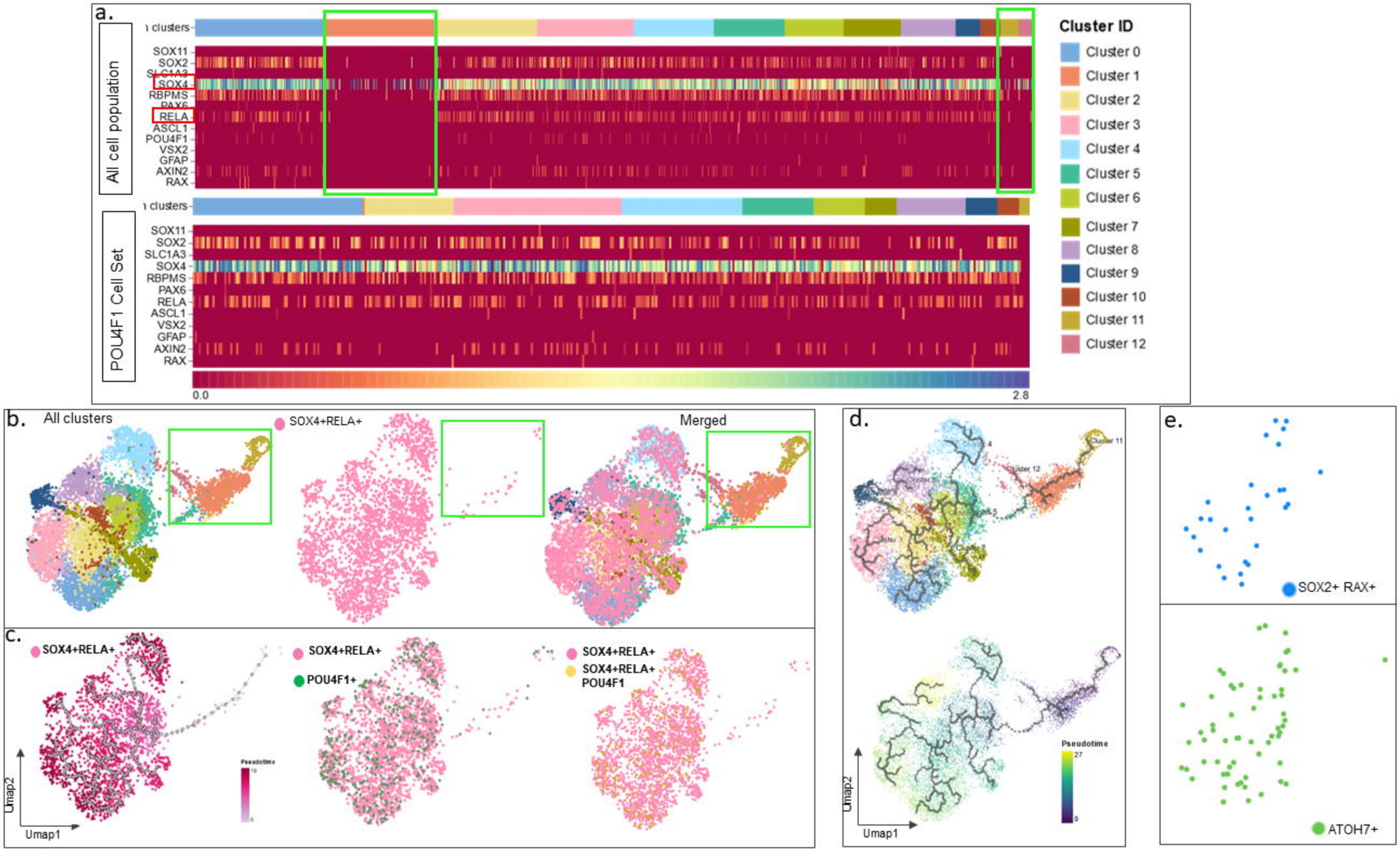

Extended data Fig.12

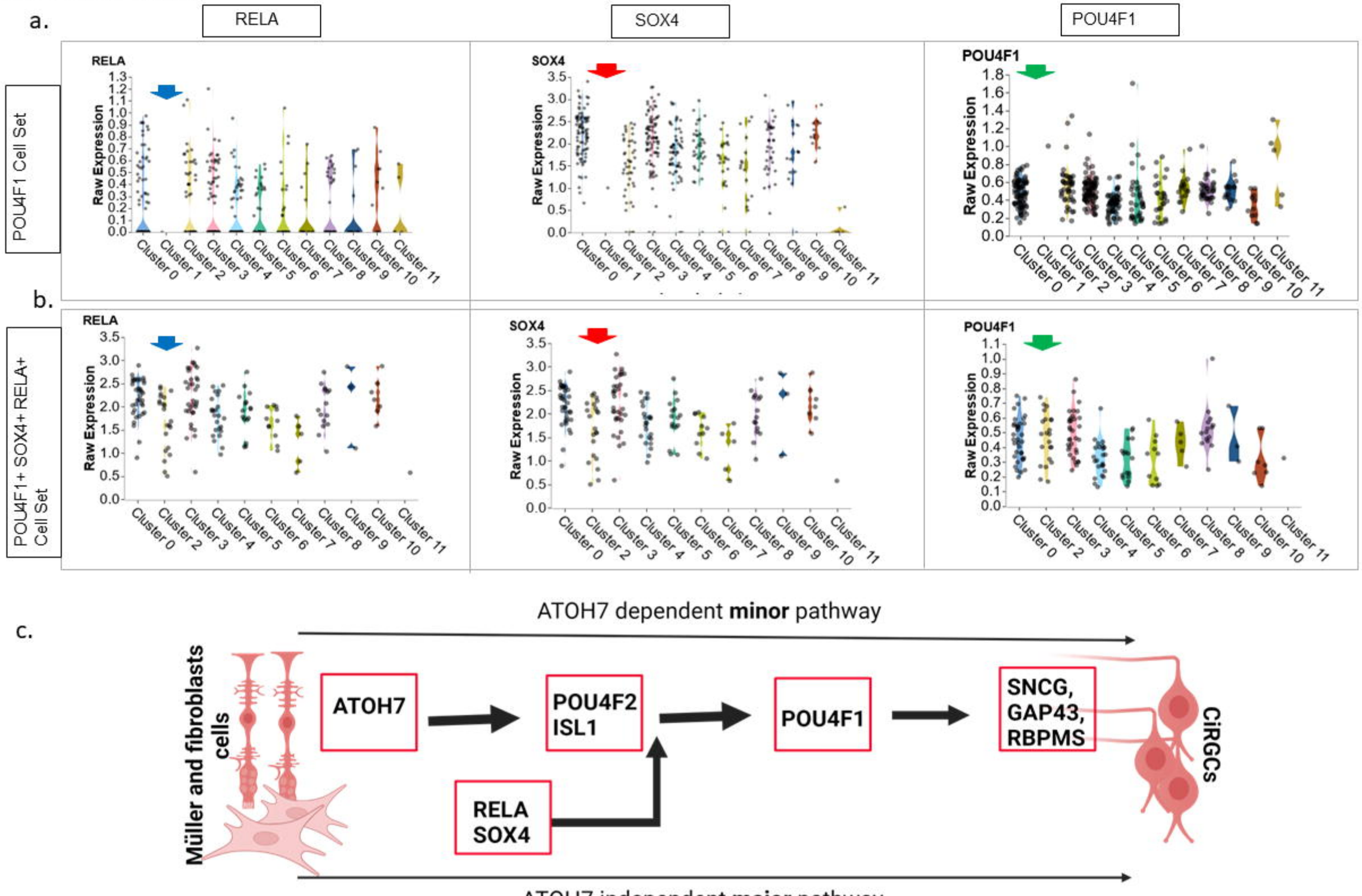

Extended data Fig.13

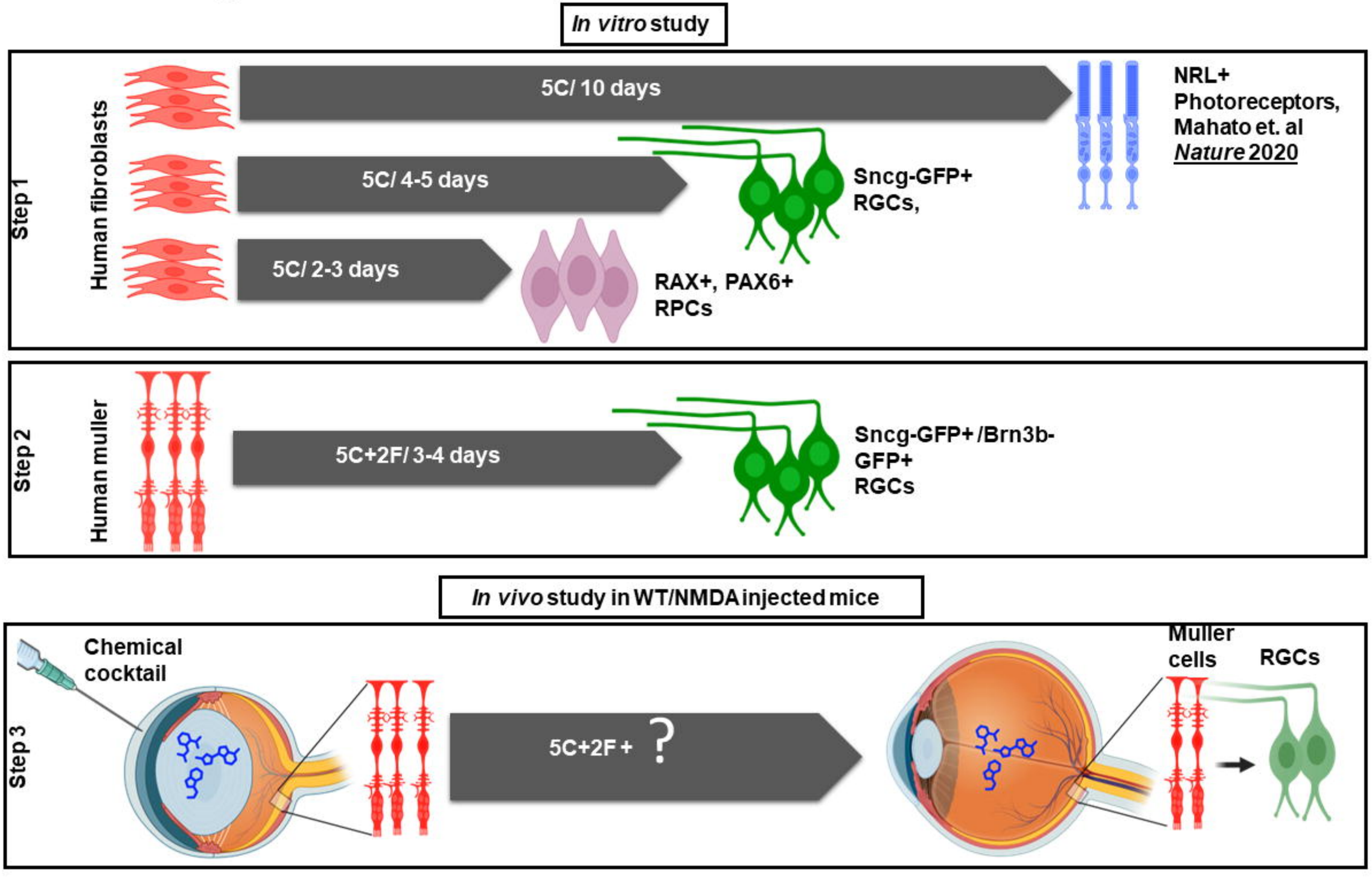

Extended data Fig.14

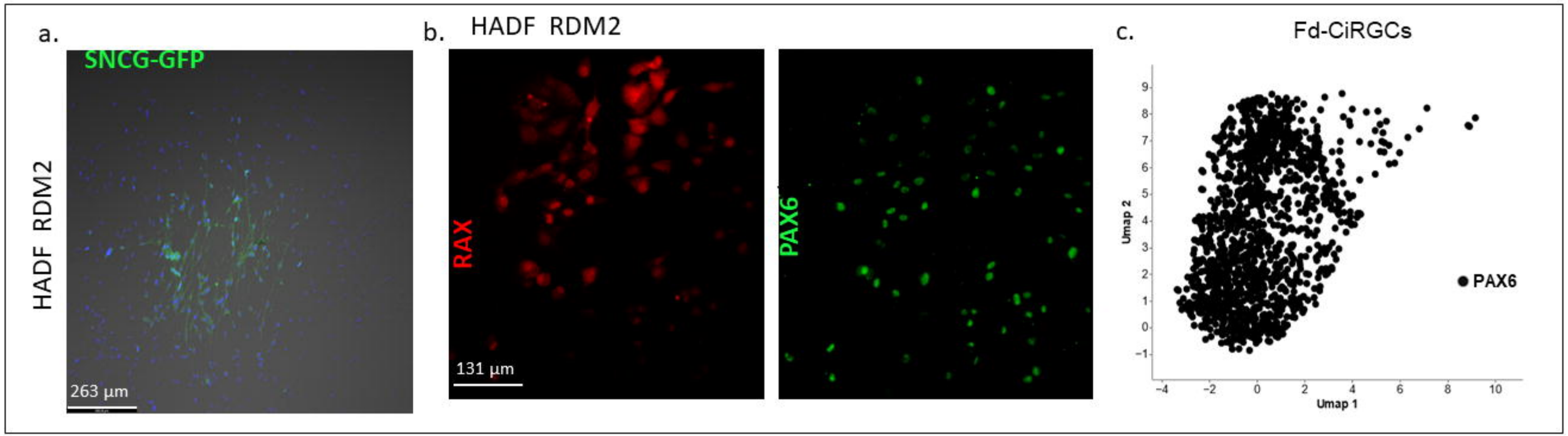

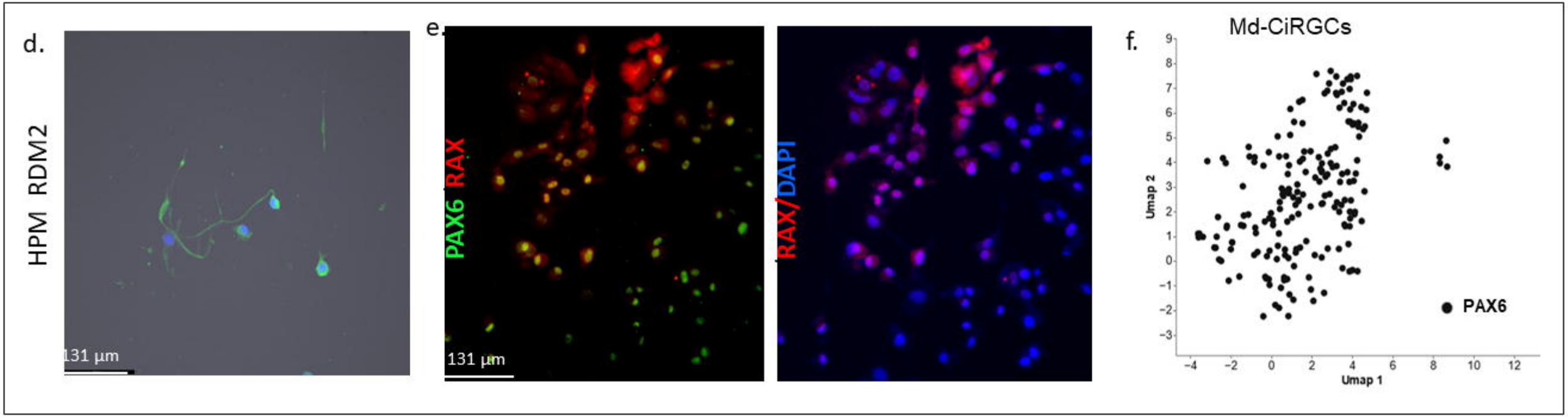

Extended data Fig. 15

a.

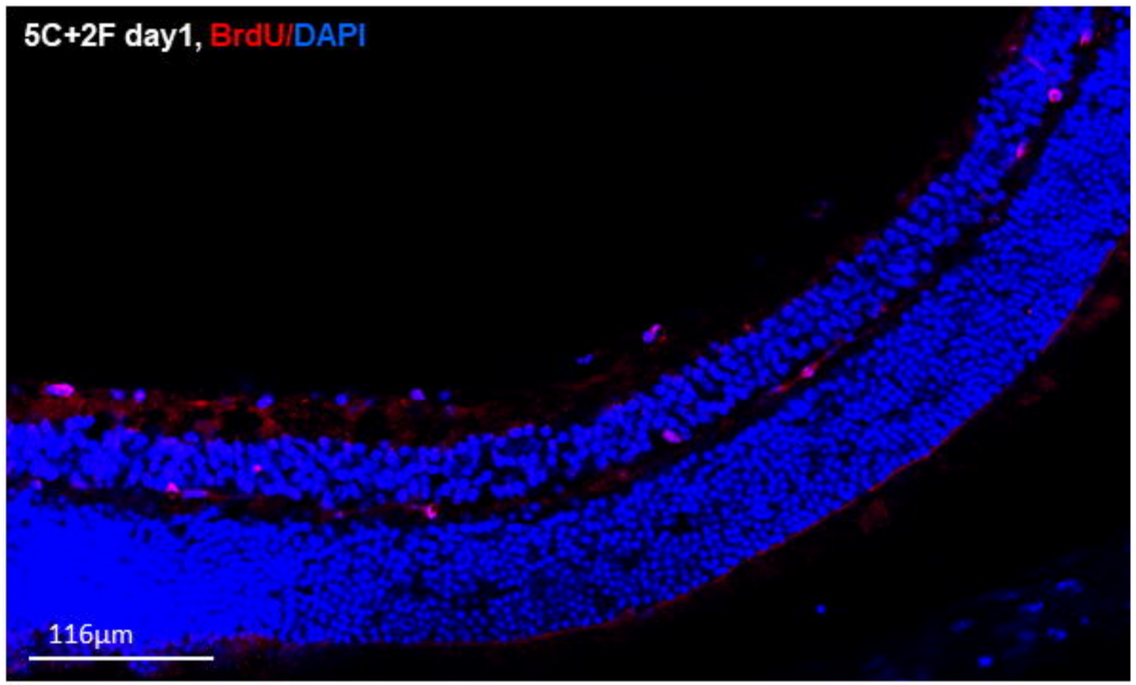
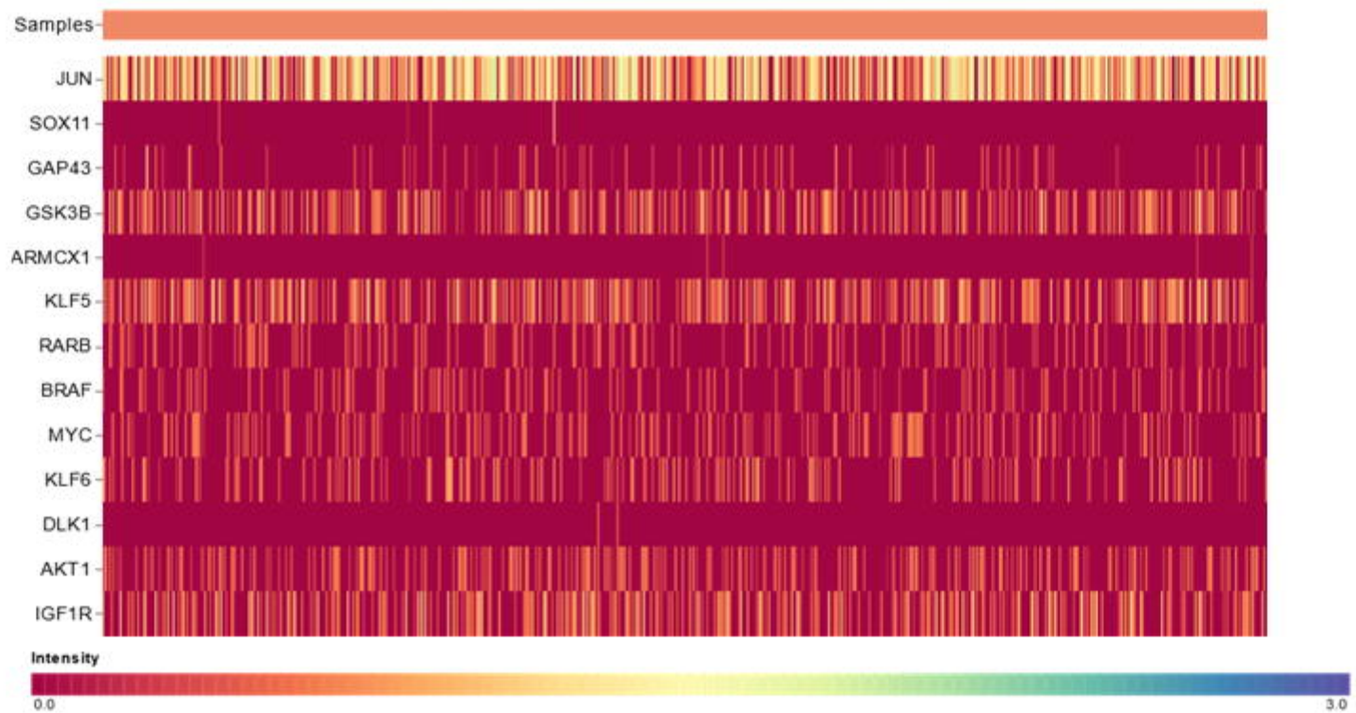
b.